A&A 461, 823–845 (2007)
DOI: 10.1051/0004-6361:20053941

Astronomy & Astrophysics

Protoclusters associated with $z > 2$ radio galaxies[⋆,⋆⋆]

I. Characteristics of high redshift protoclusters

B. P. Venemans[1,2], H. J. A. Röttgering[1], G. K. Miley[1], W. J. M. van Breugel[3,8], C. De Breuck[4], J. D. Kurk[5], L. Pentericci[6], S. A. Stanford[3,9], R. A. Overzier[1], S. Croft[3,8], and H. Ford[7]

[1] Sterrewacht Leiden, PO Box 9513, 2300 RA, Leiden, The Netherlands
[2] Institute of Astronomy, University of Cambridge, Madingley Road, Cambridge, CB3 0HA, UK
e-mail: venemans@ast.cam.ac.uk
[3] Lawrence Livermore National Laboratory, PO Box 808, Livermore CA, 94550, USA
[4] European Southern Observatory, Karl Schwarzschild Straße 2, 85748 Garching, Germany
[5] INAF, Osservatorio Astrofisico di Arcetri, Largo Enrico Fermi 5, 50125, Firenze, Italy
[6] Osservatorio Astronomico di Roma, Via di Frascati 33, 00040 Monte Porzio Catone, Italy
[7] Dept. of Physics & Astronomy, The Johns Hopkins University, 3400 North Charles Street, Baltimore MD, 21218-2686, USA
[8] University of California, Merced, PO Box 2039, Merced, CA 95344, USA
[9] University of California, Davis, 1 Shields Ave, Davis, CA 95616, USA

Received 29 July 2005 / Accepted 5 October 2006

ABSTRACT

We present the results of a large program conducted with the Very Large Telescope and augmented by observations with the Keck telescope to search for forming clusters of galaxies near powerful radio galaxies at $2.0 < z < 5.2$. Besides MRC 1138−262 at $z = 2.16$, the radio galaxy observed in our pilot program, we obtained narrow- and broad-band images of eight radio galaxies and their surroundings. The imaging was used to select candidate Lyα emitting galaxies in ∼3×3 Mpc^2 areas near the radio galaxies. A total of 300 candidate emitters were found with a rest-frame Lyα equivalent width of $EW_0 > 15$ Å and significance $\Sigma \equiv EW_0/\Delta EW_0 > 3$. Follow-up spectroscopy was performed on 152 candidates in seven of the radio galaxy fields. Of these, 139 were confirmed to be Lyα emitters, four were low redshift interlopers and nine were non-detections. With the adopted criteria the success rate is 139/152 = 91%. In addition, 14 objects with $EW_0 < 15$ and/or $\Sigma < 3$ were confirmed to be Lyα emitters. Combined with the 15 Lyα emitters near MRC 1138−262, we have determined Lyα redshifts for 168 objects near eight radio galaxies.
At least six of our eight fields are overdense in Lyα emitters by a factor 3−5 as compared to the field density of Lyα emitters at similar redshifts, although the statistics in our highest redshift field ($z = 5.2$) are poor. Also, the emitters show significant clustering in velocity space. In the overdense fields, the width of the velocity distributions of the emitters is a factor 2−5 smaller than the width of the narrow-band filters. Taken together, we conclude that we have discovered six forming clusters of galaxies (protoclusters). We estimate that roughly 75% of powerful ($L_{2.7\,\mathrm{GHz}} > 10^{33}$ erg s^{-1} Hz^{-1} sr^{-1}) high redshift radio galaxies reside in a protocluster. The protoclusters have sizes of at least 1.75 Mpc, which is consistent with the structure sizes found by other groups. By using the volume occupied by the overdensities and assuming a bias parameter of $b = 3$−6, we estimate that the protoclusters have masses in the range $2{-}9{\times}10^{14}$ $M_\odot$. These protoclusters are likely to be progenitors of present-day (massive) clusters of galaxies. For the first time, we have been able to estimate the velocity dispersion of cluster progenitors from $z \sim 5$ to ∼2. The velocity dispersion of the emitters increases with cosmic time, in agreement with the dark matter velocity dispersion in numerical simulations of forming massive clusters.

Key words. galaxies: active – galaxies: clusters: general – cosmology: observations – cosmology: early Universe – cosmology: large scale structure of Universe

1. Introduction

Clusters of galaxies are the largest and most massive gravitationally bound structures in the Universe. They are interesting objects to study for many reasons.

First, clusters contain large numbers of galaxies at specific redshifts, making them excellent laboratories with which to investigate the formation and evolution of galaxies. For example, the analysis of galaxies in $z \sim 1$ clusters showed that the stars in massive, early-type galaxies formed at $z > 2$ (e.g., Ellis et al. 1997; Stanford et al. 1998; Blakeslee et al. 2003; van Dokkum & Stanford 2003; Holden et al. 2005). Investigating the galaxy population of (forming) clusters at $z > 2$ could provide knowledge of the formation process of such massive galaxies (e.g., Eggen et al. 1962; Larson 1974). Also because clusters are the most extreme overdense regions in the Universe, they allow an efficient investigation of the interaction between galaxies and their environment (e.g., Miles et al. 2004; Tanaka et al. 2004; van Zee et al. 2004; Goto 2005; Nakata et al. 2005; Tran et al. 2005).

A second reason to study clusters is that they can place constraints on cosmology. The number density of massive clusters is a strong function of the fundamental cosmological parameters Ω_M and σ_8, and the evolution of cluster abundances with redshift depends primarily on Ω_M (e.g., Eke et al. 1996). The number density of rich clusters at $z > 0.5$ has already been

⋆ Based on observations carried out at the European Southern Observatory, Paranal, Chile, programs 66.A-0597, LP167.A-0409, 68.B-0295 and 70.A-0589. Also based on data obtained at the W.M. Keck Observatory, which is operated as a scientific partnership among the California Institute of Technology, the University of California and the National Aeronautics and Space Administration. The Observatory was made possible by the generous financial support of the W.M. Keck Foundation.

⋆⋆ Appendix A is only available at http://www.aanda.org

successfully used to constrain the values of cosmological parameters (e.g., Bahcall et al. 1997; Bahcall & Fan 1998; Ettori et al. 2003).

Several studies of massive clusters with redshifts up to $z = 1.4$ have found little evolution in the cluster properties (e.g., Tozzi et al. 2003; Hashimoto et al. 2004; Maughan et al. 2004; Rosati et al. 2004; Mullis et al. 2005). Despite the large lookback times, clusters at $z \sim 1$ appear to be very similar to local clusters. For example, the $z = 1.3$ cluster RDCS 1252.9-2927 has thermodynamical properties and metallicity that are very similar to those of lower redshift clusters (Rosati et al. 2004). To study when and how clusters and their galaxies formed, a sample of clusters at $z \gg 1$ is needed.

Unfortunately, conventional methods for finding distant clusters become impractical at $z > 1$. Searches for extended X-ray sources are difficult because the surface brightness of the X-ray emission fades as $(1 + z)^4$. Although large optical surveys have been successful in finding galaxy clusters at $z \lesssim 1$ by searching for concentrations of red galaxies (e.g., Gladders 2002), the detection of $z > 1$ clusters with the same method requires sensitive, wide field near-infrared cameras which are not yet available. In the future, surveys exploiting the Sunyaev-Zeldovich (SZ) effect (e.g., Carlstrom et al. 2002) will be able to detect clusters of galaxies at $z \gg 1$. However, at this moment the sensitivity of SZ surveys is not sufficient to detect any of the known clusters at $z > 1$ (Carlstrom et al. 2002; Rosati et al. 2004). In recent years, several distant forming clusters (protoclusters) have been serendipitously discovered in field surveys (e.g., Steidel et al. 1998, 2005; Shimasaku et al. 2003; Ouchi et al. 2005). For example, Steidel et al. (1998) found a large scale structure of Lyman Break galaxies (LBGs) at $z \sim 3.1$ in one of their fields. This single discovery demonstrated the power of such structures as it could be derived that LBGs must be very biased tracers of mass.

A different approach to find (forming) clusters is to search for a galaxy concentration near a presumed tracer of high density regions. There is considerable evidence that powerful high redshift radio galaxies might be such tracers, as they are forming massive galaxies in dense environments (e.g., Carilli et al. 1997; Dey et al. 1997; Athreya et al. 1998; Pentericci et al. 1998; Papadopoulos et al. 2000; Pentericci et al. 2000b; Archibald et al. 2001; Jarvis et al. 2001; De Breuck et al. 2002, 2003a,b; Stevens et al. 2003; Zirm et al. 2003; Reuland et al. 2004; see e.g. Carilli et al. 2001 for a review). Targeted searches for companion galaxies near powerful radio sources at $z > 1$ have long yielded promising results (e.g., Le Fèvre et al. 1996; Pascarelle et al. 1996; Keel et al. 1999; Sánchez & González-Serrano 1999, 2002; Best 2000; Hall et al. 2001; Nakata et al. 2001; Best et al. 2003; Wold et al. 2003; Barr et al. 2004).

We therefore started a large program with the Very Large Telescope (VLT) to systematically search for galaxy overdensities near radio galaxies in the redshift range $2 < z < 5.2$. This program was initiated after a successful pilot project in which the environment of the radio galaxy MRC 1138–262 at $z = 2.16$ was investigated. Deep narrow-band images of the radio galaxy and the surrounding field were obtained to search for an excess of Lyα emitting galaxies (Kurk et al. 2000). The imaging and follow-up spectroscopy resulted in ~40 candidate Lyα emitters (Kurk et al. 2000, 2004b) of which 15 were confirmed at $z = 2.16 \pm 0.02$ (Pentericci et al. 2000a; Croft et al. 2005). The presence of a forming cluster associated with MRC 1138–262 was firmly established by the subsequent discovery of significant populations of (spectroscopically-confirmed) Hα emitters (Kurk et al. 2004a,b), QSOs (Pentericci et al. 2002; Croft et al. 2005) and extremely red objects (Kurk et al. 2004b). The VLT large program was augmented by observations with the Keck telescope, to take advantage of the excellent UV throughput of LRIS-B for spectroscopy and imaging below the Lyman break of some of the $z \sim 3$ objects.

In this paper, we present the results of our program to search for forming clusters (protoclusters) near radio galaxies up to $z = 5.2$. Early results of the program, the discovery of galaxy overdensities at $z = 4.1$ and $z = 5.2$, have been presented in Venemans et al. (2002) and in Venemans et al. (2004). A detailed analysis of the field towards the radio galaxy MRC 0316–257 at $z = 3.13$ is given in Venemans et al. (2005, hereafter V05). In V05 the data reduction steps, selection procedure of candidate Lyα emitters and the assessment of the data quality are described in detail. Here we will follow the same steps as V05 for the data reduction and analysis of the other fields. While in this paper we will focus on the environment of radio galaxies, in the second paper of this series we will describe the properties of the individual Lyα emitting galaxies discovered in our program.

The structure of this paper is as follows: in Sect. 2.1 we present the targets of our program, and in Sects. 2.2–2.4 we give the details of the imaging observations, the selection of candidate Lyα emitters and follow-up spectroscopy. In Sect. 3, the results of the imaging and spectroscopy are described for each individual field. A summary of the results and the evidence for the presence of protoclusters near the radio galaxies are given in Sect. 4. The properties of the protoclusters are presented in Sect. 5, followed by a discussion of our results in Sect. 6 and a summary in Sect. 7.

In this article, we adopt a Λ-dominated cosmology with $H_0 = 70\ \mathrm{km\,s^{-1}\,Mpc^{-1}}$, $\Omega_\mathrm{M} = 0.3$, and $\Omega_\Lambda = 0.7$. Magnitudes are given in the AB system (Oke 1974).

2. Observations

2.1. Sample selection

The targets for our program were selected from a list of approximately 150 radio galaxies with known redshifts of $z > 2$. Our targets were chosen to have large radio luminosities ($L_{2.7\ \mathrm{GHz}} > 10^{33}\ \mathrm{erg\,s^{-1}\,Hz^{-1}\,sr^{-1}}$). Because our goal was to search for companion Lyα emitting galaxies near the radio sources, the radio galaxies had to have redshifts optimum for imaging with the narrow-band filters that were available at the VLT. Also, the radio sources need to lie in the southern hemisphere ($\delta \lesssim 0°$) to allow deep imaging of the source with the VLT. Applying these criteria to the list of ~150 $z > 2$ radio sources reduced the number of possible targets for our program to 16 of which nine are at $z \sim 2.1$ (this includes the target of our pilot project, MRC 1138−262 at $z = 2.16$), three are at $z \sim 2.9$ and four are at $z \sim 3.1$. Given the relatively small number of radio sources at $z > 2.9$ that could be observed with the VLT, we did not apply other criteria. To extend the redshift range, we purchased narrow-band filters that were centred on the wavelength of the Lyα line at a redshift of $z = 4.1$ and $z = 5.2$. The following nine radio sources were chosen as targets for our program: BRL 1602−174 (hereafter 1602), MRC 2048−272 (2048) and MRC 1138−262 (1138, all three at $z = 2.1$), MRC 0052–241 (0052) and MRC 0943–242 (0943, both at $z = 2.9$), MRC 0316–257 (0316) and TN J2009–3040 (2009, both at $z = 3.1$), TN J1338–1942 (1338, $z = 4.1$) and TN J0924–2201 (0924, $z = 5.2$). Because these targets were selected only on the basis of their radio luminosity and position on the sky, we regard our sample as representative of luminous radio sources. The position, redshift and radio power of the

Table 1. Details of the radio galaxies observed in our program.

Name	α_{J2000}	δ_{J2000}	z	$L^a_{2.7\ \mathrm{GHz}}$
BRL 1602–174	16 05 01.7	−17 34 18.4	2.04	2.0×10^{34}
MRC 2048–272	20 51 03.5	−27 03 04.1	2.06	6.3×10^{33}
MRC 1138–262	11 40 48.2	−26 29 09.5	2.16	1.3×10^{34}
MRC 0052–241	00 54 29.8	−23 51 31.1	2.86	8.6×10^{33}
MRC 0943–242	09 45 32.7	−24 28 49.7	2.92	7.2×10^{33}
MRC 0316–257	03 18 12.0	−25 35 10.8	3.13	1.4×10^{34}
TN J2009–3040	20 09 48.1	−30 40 07.4	3.16	2.8×10^{33}
TN J1338–1942	13 38 26.1	−19 42 30.8	4.11	9.6×10^{33}
TN J0924–2201	09 24 19.9	−22 01 42.0	5.20	1.5×10^{34}

[a] Radio luminosity at a rest-frame frequency of 2.7 GHz in erg s^{-1} Hz^{-1} sr^{-1}.

targets are given in Table 1. Individual radio galaxies are briefly described in Sect. 3.

2.2. Imaging observations

To search for structures of Lyα emitting galaxies near the radio galaxies, the fields surrounding the radio galaxies were observed in a narrow-band filter and at least one broad-band filter. The narrow-band filters were chosen to encompass the Lyα line at the redshift of the radio galaxy, and the broad-band filters were selected to measure the UV continuum redward of the Lyα line.

All the narrow-band imaging and most of the broad-band imaging obtained in the large program were performed with the FOcal Reducer/low dispersion Spectrograph 2 (FORS2; Appenzeller & Rupprecht 1992) in imaging mode. Before 2002 April, the detector in FORS2 was a SiTE CCD with 2048×2048 pixel^2 and a pixel scale of 0.″2 pixel^{-1}. In 2002 April, the SiTE CCD was replaced by two MIT CCDs each with 2048×2048 pixel^2 with a scale of 0.″125 pixel^{-1}. The pixels were binned by 2×2, which decreases the readout time by a factor of 2 and gives a pixels scale of 0.″25 pixel^{-1}. The field of view, which is restricted by the geometry of the Multi-Object Spectroscopy unit, is 6.′8 × 6.′8.

Additional (broad-band) imaging was obtained using the Low Resolution Imaging Spectrometer (LRIS, Oke et al. 1995) on the Keck I telescope. LRIS has two arms: a blue channel which is optimised for observations in the blue part of the optical spectrum (LRIS-B, see McCarthy et al. 1998; Steidel et al. 2004, for more information) and a red channel for observing in the red (LRIS-R, Oke et al. 1995). The red arm is equipped with a Tektronix CCD with 2048 × 2048 pixel^2. The pixel scale is 0.″21 pixel^{-1}, resulting in a field of view of 7.′3×7.′3. The blue channel has two 2048×4096 Marconi CCDs with a pixel scale of 0.″135 pixel^{-1}. There is a small gap between the CCDs of roughly 13.″5. The field of view is ∼8′×8′[1].

Observations were split into separate exposures of typically 1200−1800 s in the narrow-band and 240−800 s in the broad-band. Individual exposures were shifted 10″−15″ with respect to each other to facilitate the identification of cosmic rays and the removal of residual flat-field errors. The data were reduced using standard routines within the reduction software package IRAF[2]. These routines included bias subtraction using either bias frames or the overscan region of the CCD, flat fielding with twilight sky flats and illumination correction using the unregistered science frames.

All science images were registered on the ICRF astrometric frame of reference (Ma & Feissel 1998), using the USNO-A2.0 catalogue (Monet et al. 1998; Monet 1998). The relative positions of objects in the fields are accurate to 0.″1−0.″2. The absolute accuracy is dominated by the uncertainty in the USNO-A2.0 catalogue of 0.″25 (Deutsch 1999).

The photometric calibration was performed using several photometric and spectrophotometric standard stars from the catalogues of Stone & Baldwin (1983), Baldwin & Stone (1984), Oke (1990) and Landolt (1992). The magnitude zero-points derived from these standard stars are consistent with each other within 2−3%. Zero-points in the Vega system are converted to the AB system using the transformations of Bessell (1979) and Smith et al. (2002). The zero-points were corrected for galactic extinction as estimated by Schlegel et al. (1998).

Table 2 summarizes the imaging observations of our Large Program targets and gives the properties of the narrow- and broad-band filters that were used. Also, the image quality (seeing) and depth (in 1σ limiting magnitudes per square arcsecond) are given in Table 2.

2.3. Candidate selection

Objects in the images were detected using the program SExtractor (Bertin & Arnouts 1996). The narrow-band images were taken to detect objects, and aperture photometry was subsequently performed on both the narrow-band and the broad-band images.

To assess the completeness of the source detection, artificial and real point sources were added to the narrow-band image and recovered. The completeness limit was defined as the narrow-band magnitude at which 50% of the added sources was recovered (see V05 for details).

Detected objects were required to have a signal-to-noise of >5 in the narrow-band image. The colors of the detected objects were measured in circular apertures, while the "total" flux was measured in an elliptical aperture. A correction was made to the "total" flux to account for the flux outside the elliptical aperture. More details on the object detection, completeness assessment, aperture sizes for the photometry and "total" flux correction can be found in V05.

Following Venemans et al. (2002) and V05, we selected objects with a rest-frame equivalent width $EW_0 > 15$ Å and a significance $\Sigma \equiv EW_0/\Delta EW_0 > 3$ as good candidate Lyα emitters. In V05 a detailed description is presented on how EW_0 and ΔEW_0 are computed from the available photometry. For two fields that are imaged in at least two broad-band filters, the 0316 and 0052 fields, the UV continuum slope β ($f_\lambda \propto \lambda^\beta$) of candidate emitters was also computed. For the other fields, a "flat" continuum slope $\beta = -2$ was used to select the candidates, which is close to the median β of confirmed Lyα emitters in the 0316 field ($\beta = -1.76$, V05). In each field the candidate emission line galaxies were visually inspected and spurious sources (like spikes of bright, saturated stars) were removed from the catalogues. The resulting lists should have a very low fraction of contaminants, such as low redshift interlopers (∼5% as esimated by V05).

In Table 3 the 50% completeness limit, number of candidate emitters and area of each observed field is listed. We also

[1] The specifications for the blue channel detectors given here apply for data taken after 2002 June.

[2] IRAF is distributed by the National Optical Astronomy Observatories, which are operated by the Association of Universities for Research in Astronomy, Inc., under cooperative agreement with the National Science Foundation.

Table 2. Overview of the imaging observations of the radio galaxy fields.

Date	Telescope	Instrument	Field	Filter	$\lambda_c{}^a$ (Å)	$\Delta\lambda^b$ (Å)	Seeing	$t^c_{\rm exp}$	Depth^d
2001 Mar. 24 & 25	VLT UT2	FORS2	1338-1^e	FILT_621_5	6199	59	0.″6	33 300	28.2
2001 Mar. 24 & 25	VLT UT2	FORS2	1338-1^e	Special *R*	6550	1650	0.″6	6300	28.9
2001 Mar. 24–26	VLT UT2	FORS2	0943	HeII/6500	4781	68	0.″7	22 500	28.6
2001 Mar. 25 & 26	VLT UT2	FORS2	0943	Bessel *B*	4290	880	0.″9	4500	28.7
2001 Mar. 25 & 26	VLT UT2	FORS2	1602	OII	3717	73	0.″8	15 000	26.6
2001 Mar. 26	VLT UT2	FORS2	1602	Bessel *B*	4290	880	0.″65	2700	27.6
2001 May 21–23	VLT UT2	FORS2	2048	OII	3717	73	0.″95	25 200	–^{f}
2001 May 22 & 23	VLT UT2	FORS2	2048	Bessel *B*	4290	880	1.″05	3600	–^{f}
2001 Sep. 20–22	VLT UT4	FORS2	2048	OII	3717	73	0.″95	25 200	27.9
2001 Sep. 20 & 21	VLT UT4	FORS2	2048	Bessel *B*	4290	880	1.″05	3000	28.8
2001 Sep. 20 & 21	VLT UT4	FORS2	0316	OIII/3000	5045	59	0.″7	23 400	28.4
2001 Sep. 20 & 21	VLT UT4	FORS2	0316	Bessel *V*	5540	1115	0.″7	4860	28.9
2001 Sep. 22	VLT UT4	FORS2	0052	HeII	4684	66	0.″75	5400	–^{f}
2001 Oct. 20	VLT UT4	FORS2	0052	HeII	4684	66	0.″75	18 000	28.3
2001 Oct. 20	VLT UT4	FORS2	0052	Bessel *B*	4290	880	0.″8	4800	29.0
2002 Mar. 8	VLT UT4	FORS2	0924	FILT_753_8	7528	89	0.″8	14 400	–^{f}
2002 Mar. 8	VLT UT4	FORS2	0924	Bessel *I*	7680	1380	0.″8	2700	–^{f}
2002 Apr. 17–19	VLT UT4	FORS2	0924	FILT_753_8	7528	89	0.″8	28 800	28.1
2002 Apr. 17–19	VLT UT4	FORS2	0924	Bessel *I*	7680	1380	0.″8	8640	28.5
2002 Apr. 17–19	VLT UT4	FORS2	1338-2^e	FILT_621_5	6199	59	0.″75	25 200	28.2
2002 Apr. 17–19	VLT UT4	FORS2	1338-2^e	Special *R*	6550	1650	0.″75	4500	28.9
2002 Apr. 17–19	VLT UT4	FORS2	2009	OIII/3000	5045	59	0.″9	21 600	–^{f}
2002 Apr. 17–19	VLT UT4	FORS2	2009	Bessel *V*	5540	1115	0.″85	4800	–^{f}
2002 Apr. 19	VLT UT4	FORS2	0924	Bessel *V*	5540	1115	1.″05	3600	28.6
2002 Sep. 6–8	VLT UT4	FORS2	0316	Bessel *I*	7680	1380	0.″7	4680	28.7
2002 Sep. 8	VLT UT4	FORS2	2009	OIII/3000	5045	59	0.″9	7200	28.0
2002 Sep. 8	VLT UT4	FORS2	2009	Bessel *V*	5540	1115	0.″85	2400	28.6
2002 Sep. 8	VLT UT4	FORS2	0052	Bessel *V*	5540	1115	0.″75	5400	29.2
2002 Sep. 8	VLT UT4	FORS2	0052	Bessel *I*	7680	1380	0.″55	4800	28.5
2003 Jan. 31	Keck I	LRIS-B	0316	u'	3550	600	1.″25	4050	–^{f}
2003 Feb. 1 & 4	Keck I	LRIS-B	0316	u'	3550	600	1.″25	9000	29.8
2003 Feb. 4	Keck I	LRIS-B	0943	u'	3550	600	1.″2	9600	–^{f}
2003 Feb. 4	Keck I	LRIS-R	0943	*V*	5473	948	1.″25	5600	29.4
2004 Jan. 19	Keck I	LRIS-B	0943	u'	3550	600	1.″2	7000	29.8
2004 Jan. 19	Keck I	LRIS-R	0943	*I*	8331	3131	0.″90	6000	28.4

[a] Central wavelength of the filter in Å.
[b] Full width at half maximum (*FWHM*) of the filter in Å.
[c] Total exposure time in seconds.
[d] 1σ depth of the resulting image in mag per □″.
[e] The field towards TN J1338–1942 was observed at two different pointings, see Sect. 3.8.
[f] For images obtained during two different observing sessions, only the total depth is listed in the final entry.

calculated the 5σ limiting line flux and line luminosity of an emitter with a negligible continuum. The number of candidates in the 1138 field is taken from Kurk et al. (2004b).

2.4. Spectroscopic observations

To confirm whether the candidate emission line objects are located at the redshift of the radio galaxy, spectra were taken of candidate emitters. Priority was given to the most luminous candidates. In Table 4 a summary is given of the spectroscopic observations of candidate emitters in the radio galaxy fields.

Most of the spectroscopic observations were performed using user-defined masks (the multi-object spectroscopy (MXU) mode of FORS2 and multi-slit spectroscopy (MSS) modes of LRIS in Table 4). This mode allowed us to observe between 20 and 40 objects per slitmask. The slits typically had a length of 10″−12″ and a width of 1.″0−1.″4. The grisms used were selected to have the highest throughput at the wavelength of the Lyα line of the radio galaxy and a resolution that matches the width of the Lyα lines (∼300 km s^{-1}, V05) to maximize the confirmation rate.

Individual exposures were typically 1800−2700 s, which ensured that the spectra were limited by the sky noise. Between the exposures the pointing of the telescope was shifted 2″−5″ along the slits to enable more accurate sky subtraction. For the flux calibration long slit exposures of (at least) one of the following spectroscopic standard stars EG 274, Feige 67, Feige 110, GD 108, LTT 377, LTT 1020, LTT 1788, LTT 6248 and LTT 7987 (Stone & Baldwin 1983; Baldwin & Stone 1984; Oke 1990) were used. The flux calibration is accurate to about ∼5%. This does not take into account the uncertainties due to slit losses. Because we calculated the total flux of the emission lines using the imaging photometry, we did not attempt to correct the spectra for flux falling outside the slit.

The details of the reduction of the spectroscopic data is given in V05. In the next section, we will describe the results in the individual fields.

Table 3. Depth, sensitivity and size of the imaging observations of the radio galaxies fields, and the number of candidates selected in each field.

Field	$m^a_{\rm lim}$	$F^b_{5\sigma}$ erg s^{-1} cm^{-2}	$L^c_{5\sigma}$ erg s^{-1}	N^d	Area^e arcmin^2
1602	24.4	9.7×10^{-17}	3.4×10^{42}	2	42.3
2048	25.4	3.3×10^{-17}	1.2×10^{42}	10	43.6
1138	25.2^f	3.5×10^{-17} ^{f}	1.4×10^{42} ^{f}	37^f	46.6^f
0052	26.1	1.1×10^{-17}	8.4×10^{41}	57	44.9
0943	26.1	7.4×10^{-18}	6.2×10^{41}	65	46.5
0316	26.3	6.9×10^{-18}	6.9×10^{41}	77	45.8
2009	25.7	1.3×10^{-17}	1.3×10^{42}	21	46.7
1338-1	26.0	4.7×10^{-18}	8.9×10^{41}	31^g	40.1
1338-2	26.2	5.8×10^{-18}	1.1×10^{42}	33^g	48.9
0924	25.5	7.0×10^{-18}	2.3×10^{42}	14	46.8

[a] Magnitude at which 50% of artificial and real point sources that were added to the narrow-band image, were recovered.
[b] Line flux of an emitter with no continuum that is detected at the 5σ level in an aperture with a diameter twice that of the seeing disc.
[c] Line luminosity of an emitter with no continuum that is detected at the 5σ level in an aperture with a diameter twice that of the seeing disc.
[d] Number of candidate Lyα emitters that fulfils the selection criteria $EW_0 > 15$ Å and $EW_0/\Delta EW_0 > 3$.
[e] Imaging area useful for selection of Lyα emitters.
[f] Values taken from Kurk et al. (2004b).
[g] The 1338-1 and 1338-2 fields overlap and have an area of 9.3 arcmin^2 in common. The total number of unique candidate emitters in the two fields is 54 in an area of 79.7 arcmin^2.

3. Results

In this section we describe the results of the imaging, candidate selections and follow-up spectroscopy of the Lyα emitters in each of the nine radio galaxy fields, followed by a description of the diffuse Lyα halos of the radio galaxies. For the details of the results in the 1138, 0316 and 0924 fields we refer to Kurk et al. (2000), Pentericci et al. (2000), Venemans et al. (2004), Kurk et al. (2004b), V05 and Croft et al. (2005). Below a brief summary of the results in these fields is given.

Redshift and Lyα line properties were measured by fitting a Gaussian function to the emission line. If absorption features were present, a combination of a Gaussian and a Voigt absorption profile was fitted. The properties of the confirmed Lyα emitters in the various fields are summarized in Tables A.1−A.5. In the tables, the objects are ordered on increasing right ascension.

3.1. BRL 1602–174, z = 2.04

The radio source BRL 1602–174 was optically identified with a galaxy with $m_R = 21.4$ object along the radio axis. A spectrum of this galaxy yielded a redshift of 2.043 ± 0.002 based on four emission lines (Best et al. 1999). This places the Lyα line of the radio galaxy in the lowest wavelength narrow-band filter available for FORS2, the O II filter. The field was imaged for 250 min in the narrow-band and for 45 min in the B-band. Due to the high extinction towards this field ($A_B \approx 1$, Schlegel et al. 1998) and the low quantum efficiency at wavelengths < 4000 Å of the FORS2 detector, only two candidate Lyα emitters were found. No spectra were taken in this field.

3.2. MRC 2048–272, z = 2.06

MRC 2048–272 was listed in the 408 MHz Molonglo Reference Catalogue (Large et al. 1981) and identified with a $z = 2.06$ object by McCarthy et al. (1996). High resolution imaging in the infrared with the *HST* revealed three separate components within 3″ (Pentericci et al. 2001), of which the central object was identified as the radio galaxy. The surface brightness of the central object could be well fit by a de Vaucouleurs profile, indicating that a dynamically relaxed stellar population is in place in this radio galaxy (Pentericci et al. 2001).

Imaging observations
We observed the field in 2001 May under moderate seeing conditions (∼1″) for 7 h in the O II narrow-band filter and for 1 h in the B-band. Because of the low efficiency of the detector at $\lambda < 4000$ Å and the high extinction towards the field of $A_B \approx 0.4$ (Schlegel et al. 1998), the field was imaged again in 2001 September. The combined 14 h of narrow-band observations of this field have a depth comparable to that of the field surrounding MRC 1138−262 (Kurk et al. 2000, Table 3). In total 10 candidate Lyα emitters were found in this field. The number of contaminants is expected to be low in this field, because the only strong line that falls in the filter is [O II] λ3727 at a redshift of $z < 0.007$.

Spectroscopic observations
Due to geometrical constraints only three of the candidate emitters could be observed at the same time. Additional targets were included on the slitmask, including objects with a low equivalent width $EW_0 < 15$ Å. Two of the three candidates and the radio galaxy show a line in a 4 h spectrum (see Table A.1 and Fig. 1). The third emitter has most likely an emission line that is too faint ($<3 \times 10^{-17}$ erg s^{-1} cm^{-2}) to be confirmed in a 4 h spectroscopic observation with FORS2 at blue wavelengths ($\lambda \sim 3750$ Å). The two confirmed emitters have a redshift very close to that of the radio galaxy with relative velocities of 100 and 10 km s^{-1}. A third Lyα emitter was found among the candidate emitters with a lower equivalent width. This galaxy is a bright Lyα emitter located ∼4600 km s^{-1} away from the radio galaxy, with the emission line at the edge of the narrow-band filter (Fig. 1).

Volume density
Kurk et al. (2004b) found that the 1138 field is overdense in Lyα emitters by a factor of 4 ± 2 compared to the field (volume) density of Lyα emitters as derived by Stiavelli et al. (2001). Comparing the volume density of Lyα emitters near MRC 2048–272 to that of emitters near MRC 1138–262 (Kurk et al. 2004b), the density in the 2048 field is a factor $3.4^{+1.8}_{-1.2}$ smaller. The errors are based on Poisson statistics in the small numbers regime (Gehrels 1986). Using this factor, the volume density of emitters near 2048 is $1.2^{+0.8}_{-0.7}$ times the field density of emitters. A direct comparison with Stiavelli et al. (2001) gives a similar density ($n_{2048}/n_{\rm field} = 0.7^{+1.8}_{-0.6}$). The small difference between the two density estimates (at the 0.3σ level) is due the small numbers of galaxies involved in the comparison. The density in the 2048 field is consistent with no overdensity of emitters near the radio galaxy.

3.3. MRC 1138–262, z = 2.16

This radio galaxy was the target of our pilot project (see also Sect. 1). Narrow- and broad-band imaging with FORS1 on the

Table 4. Overview of the spectroscopic observations of the radio galaxy fields.

Date	Telescope	Instrument	Field	Mode[a]	Grism name	Dispersion[b]	Resolution[c]	t^d_{exp}
2001 May 20 & 22	VLT UT2	FORS2	1338-1	MXU, mask A	GRIS_600RI	1.32	$260 \times 1\farcs0$	31 500
2001 May 21 & 22	VLT UT2	FORS2	1338-1	MXU, mask B	GRIS_600RI	1.32	$265 \times 1\farcs0$	35 100
2001 Sep. 22	VLT UT4	FORS2	0316	MOS	GRIS_1400V	0.50	$130 \times 1\farcs5$	12 600
2001 Oct. 18 & 19	VLT UT4	FORS2	2048	MXU	GRIS_600B	2.40	$410 \times 1\farcs0$	16 200
2001 Oct. 18	VLT UT4	FORS2	0316	MXU, mask A	GRIS_1400V	1.00	$140 \times 1\farcs0$	10 800
2001 Oct. 18–20	VLT UT4	FORS2	0316	MXU, mask B	GRIS_1400V	1.00	$140 \times 1\farcs0$	29 100
2001 Nov. 15 & 16	VLT UT3	FORS1	0316	PMOS	GRIS_300V	2.64	$630 \times 0\farcs8$	19 800
2002 Jan. 14	Keck I	LRIS	0943	MSS, mask A	600/4000	1.01	$310 \times 0\farcs85$	10 800
2002 Jan. 15	Keck I	LRIS	0943	MSS, mask B	600/4000	1.01	$325 \times 0\farcs9$	9000
2002 Sep. 6 & 7	VLT UT4	FORS2	2009	MXU	GRIS_1400V	0.62	$110 \times 0\farcs75$	19 800
2002 Sep. 6	VLT UT4	FORS2	0052	MXU, mask A	GRIS_1400V	0.62	$100 \times 0\farcs65$	8400
2002 Sep. 6 & 7	VLT UT4	FORS2	0052	MXU, mask B	GRIS_1400V	0.62	$100 \times 0\farcs65$	17 550
2002 Sep. 7	VLT UT4	FORS2	0052	MXU, mask C	GRIS_1400V	0.62	$95 \times 0\farcs6$	10 800
2002 Sep. 8	VLT UT4	FORS2	0052	MOS	GRIS_1400V	0.62	$95 \times 0\farcs6$	9600
2003 Jan. 31	Keck I	LRIS	0943	MSS, mask C	600/4000	0.61	$205 \times 0\farcs7$	7200
2003 Feb. 1	Keck I	LRIS	0943	MSS, mask D	600/4000	0.61	$215 \times 0\farcs75$	7200
2003 Feb. 1 & 4	Keck I	LRIS	1338-2	MSS	400/8500	1.85	$320 \times 0\farcs75$	9000
2003 Mar. 3 & 4	VLT UT4	FORS2	0924	MXU	GRIS_600RI	1.66	$225 \times 0\farcs85$	20 676
2003 Mar. 4	VLT UT4	FORS2	1338-2	MXU	GRIS_1200R	0.76	$125 \times 0\farcs85$	18 600

[a] Explanation of the different observing modes:
MOS: Multi-object spectroscopy mode of FORS2, performed with 19 movable slitlets with lengths of 20″–22″.
MXU: Multi-object spectroscopy mode of FORS2 with a user-prepared mask.
PMOS: Spectropolarimetry mode of FORS1 using 9 movable slitlets of 20″.
MSS: Multi-slit spectroscopy mode of LRIS, which uses a custom laser-cut mask.
[b] Dispersion in Å pixel^{-1}.
[c] The resolution is given for both the dispersion and spatial axis. The units are [km s^{-1}] × [″].
[d] Total exposure time in seconds.

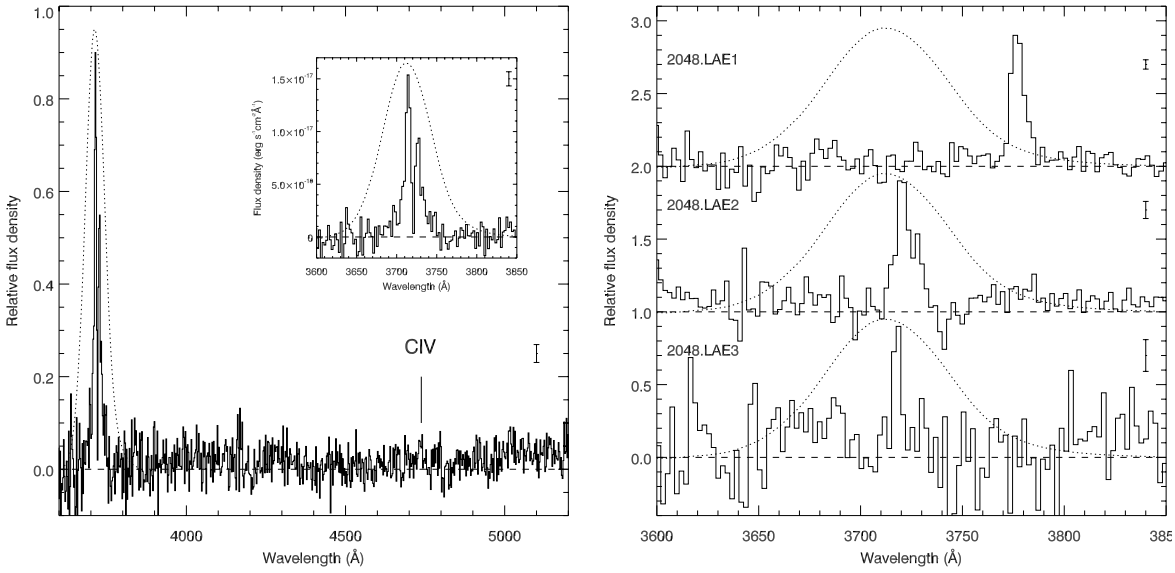

Fig. 1. Spectra of the radio galaxy MRC 2048–272 (*left*) and the three confirmed Lyα emitters near the radio galaxy (*right*). Inserted in the left plot is a close-up of the Lyα line of the radio galaxy. The dotted curve represents the transmission of the narrow-band filter that was used to select the candidate Lyα emitters. The uncertainty in the flux density is indicated by the error bar in the right corner of each spectrum.

VLT resulted in the detection of 37 candidate Lyα emitters (Kurk et al. 2000, 2004b). Subsequent spectroscopy confirmed 15 Lyα emitters to be near the radio galaxy at $z = 2.16$ (Pentericci et al. 2000a). The density of Lyα emitters in this field is roughly a factor 4 higher as compared to field studies (Pentericci et al. 2000a; Kurk et al. 2004b). This field is also overdense in X-ray sources (Pentericci et al. 2002) and extremely red objects (EROs, Kurk et al. 2004b). In total, four of the X-ray sources are confirmed to be members of the protocluster (Pentericci et al. 2002; Croft et al. 2005). Also, nine Hα emitters were spectroscopically confirmed to be associated with the radio galaxy (Kurk et al. 2004a,b), increasing the number of confirmed protocluster members to >25.

3.4. MRC 0052–241, z = 2.86

The optical counterpart of the radio source 0052–241 from the Molonglo Reference Catalogue (Large et al. 1981) was found by

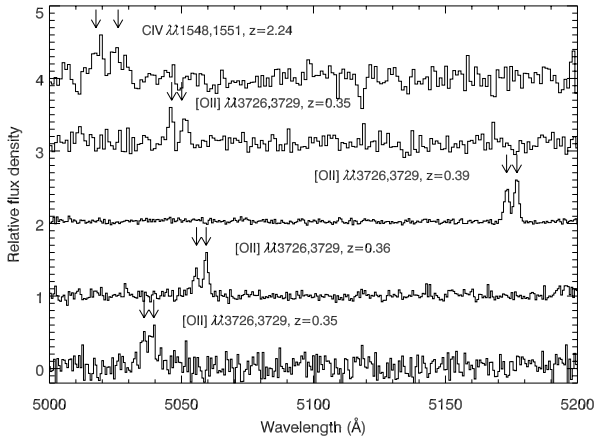

Fig. 2. Spectra of low redshift emission line galaxies which could contaminate our sample. These spectra were observed through the 1400V grism that was used for the spectroscopy observations of the 0052, 0316 and 2009 fields. Due to the resolution of $R = 2100$, interloping galaxies at low redshifts can easily be distinguished from Lyα emitters at $z \sim 3$.

McCarthy et al. (1996) to be a $m_R = 23.2$ object. A spectrum of this object showed strong Lyα emission at a redshift of $z = 2.86$ (McCarthy et al. 1996).

Imaging and spectroscopic observations

At $z = 2.86$ the Lyα line is shifted into the FORS2 narrow-band He II filter. The field was imaged for 390 min in this narrow-band and for 80, 90 and 80 min in the B-band, V-band and I-band respectively (Table 2). Analysis of these data resulted in a list of 57 candidate Lyα emitters with $EW_0 > 15$ Å and $EW_0/\Delta EW_0 > 3$ (Sect. 2.3).

Follow-up spectroscopy of candidate emitters was carried out in 2002 September at the VLT. 36 candidates were observed in four masks with individual exposure times between 140 and 292.5 min under good seeing conditions (0.″6–0.″65, see Table 4). The resolution of the grism that we used (the 1400V grism) is $R = 2100$, which is high enough to resolve the [O II] $\lambda\lambda 3726, 3729$ and C IV $\lambda\lambda 1548, 1551$ doublets (see Fig. 2 for a few examples). Objects with these emission lines in their spectrum are the main contaminants in searches for $z \sim 3$ Lyα emitters (e.g., Fynbo et al. 2003). The high resolution of the 1400V grism allows us to discriminate high redshift Lyα emitters from low redshift interlopers.

Results

Of the 36 objects observed 35 were confirmed to be Lyα emitters at a redshift $z \sim 2.86$. The 36th candidate was most likely too faint to be detected. This candidate had the smallest line flux of the objects in the mask. In addition to the 36 good candidates, four objects from a list with 20 candidate line emitters with 8 Å $< EW_0 <$ 15 Å were observed. Two of them were confirmed to be Lyα emitters at $z \sim 2.86$. One of these, emitter 0052.LAE36, has a Lyα line that falls at the red edge of the filter. Using the measured redshift ($z = 2.876$ instead of $z = 2.86$) the calculated equivalent width is $EW_0 \sim 24$ Å. The spectra of the 37 confirmed Lyα emitters and that of the radio galaxy are shown in Fig. 3.

Volume density

The density of Lyα emitters can be compared directly to the field density of emitters. Fynbo et al. (2003) used the same narrow-band filter at the VLT to observe a field which contains a damped Lyα absorber. The depth they reach in their images is approximately 0.7 mag deeper compared to our narrow-band image, making their observations suitable for comparison. Fynbo et al. (2003) find 14 emitters (of which 13 are spectroscopically confirmed) with a Lyα flux $>8 \times 10^{-18}$ erg s^{-1} cm^{-2} and a rest-frame equivalent width >15 Å. To the same limit and in the same field of view, we find 48 (candidate) emitters. This implies that the overdensity in the 0052 field is $3.4^{+1.5}_{-1.0}$.

Due to cosmic variance, the uncertainty in the number density of Lyα emitters in a small field of view like that of the VLT images is generally higher than the uncertainty derived assuming Poisson statistics (e.g., Somerville et al. 2004). To overcome this, a comparison can be made with the density of Lyα emitters at $z \sim 3.1$ in a 0.13 deg^2 field as found by Ciardullo et al. (2002). This comparison gives a volume density of Lyα emitters in the 0052 field of $2.5^{+1.8}_{-1.1}$ times the field density. The large (Poisson) errors are due to the small number statistics. More recently, Hayashino et al. (2004) measured the blank field space density of Lyα emitters at $z \sim 3.1$ using the Suprime-Cam on the Subaru telescope. In a 0.17 deg^2 field, they find 55 candidate Lyα emitters with an observed equivalent width >154 Å down to a narrow-band magnitude of 25.3. Applying the same equivalent width and magnitude criteria to our field and taking into account the difference in luminosity distance gives 11 sources. The resulting density of emitters near MRC 0052−241 is a factor $3.1^{+1.4}_{-1.0}$ higher than the field density. The weighted average of the three estimates of the overdensity is $3.0^{+0.9}_{-0.6}$.

It is interesting to compare the density of Lyα emitters in the 0052 field with the density of emitters near the radio galaxy MRC 0316−257 at $z = 3.13$ (V05). The depth and sensitivity of the imaging of the two fields are very similar (see Tables 2 and 3). There are 52 candidate emitters in the 0052 field with a narrow-band magnitude brighter than 26.1, against 59 in the 0316 field. Taking into account the difference in the volume probed by the narrow-band images, the ratio of the number density is $n_{0052}/n_{0316} = 0.8^{+0.2}_{-0.2}$. Because the 0316 field is overdense in Lyα emitters by a factor $3.3^{+0.5}_{-0.4}$ (V05), this means that the 0052 field has an overdensity of Lyα emitting galaxies of $2.7^{+0.8}_{-0.6}$, which is consistent within the errors with the other estimates.

Velocity and spatial distributions

The velocity histogram and the spatial distribution of the candidate and confirmed emitters are shown in Fig. 4. The redshifts of the confirmed emitters are not uniformly distributed throughout the narrow-band filter (solid curve in Fig. 4). Instead, the majority of the emitters (31 out of the 37) appear to be clustered in two groups with velocity dispersions of 180 and 230 km s^{-1}. Interestingly, a similar redshift distribution was found near the radio galaxy MRC 1138−262 (Pentericci et al. 2000a). The velocity of the radio galaxy lies ~70 km s^{-1} from the median redshift of the emitters and falls inside the larger of the two groups. The combination of the observed overdensity of Lyα emitters with the clumpy redshift distribution provides evidence that the Lyα emitters near MRC 0052−241 are part of a forming cluster of galaxies at $z = 2.86$. The properties of this structure will be discussed in Sect. 5.

In contrast to the velocity distribution, the emitters do not have a preferred location on the sky. The structure of emitters appears not to be bounded by the image, indicating that the overdensity seen in this field extends beyond the edges of our field of view.

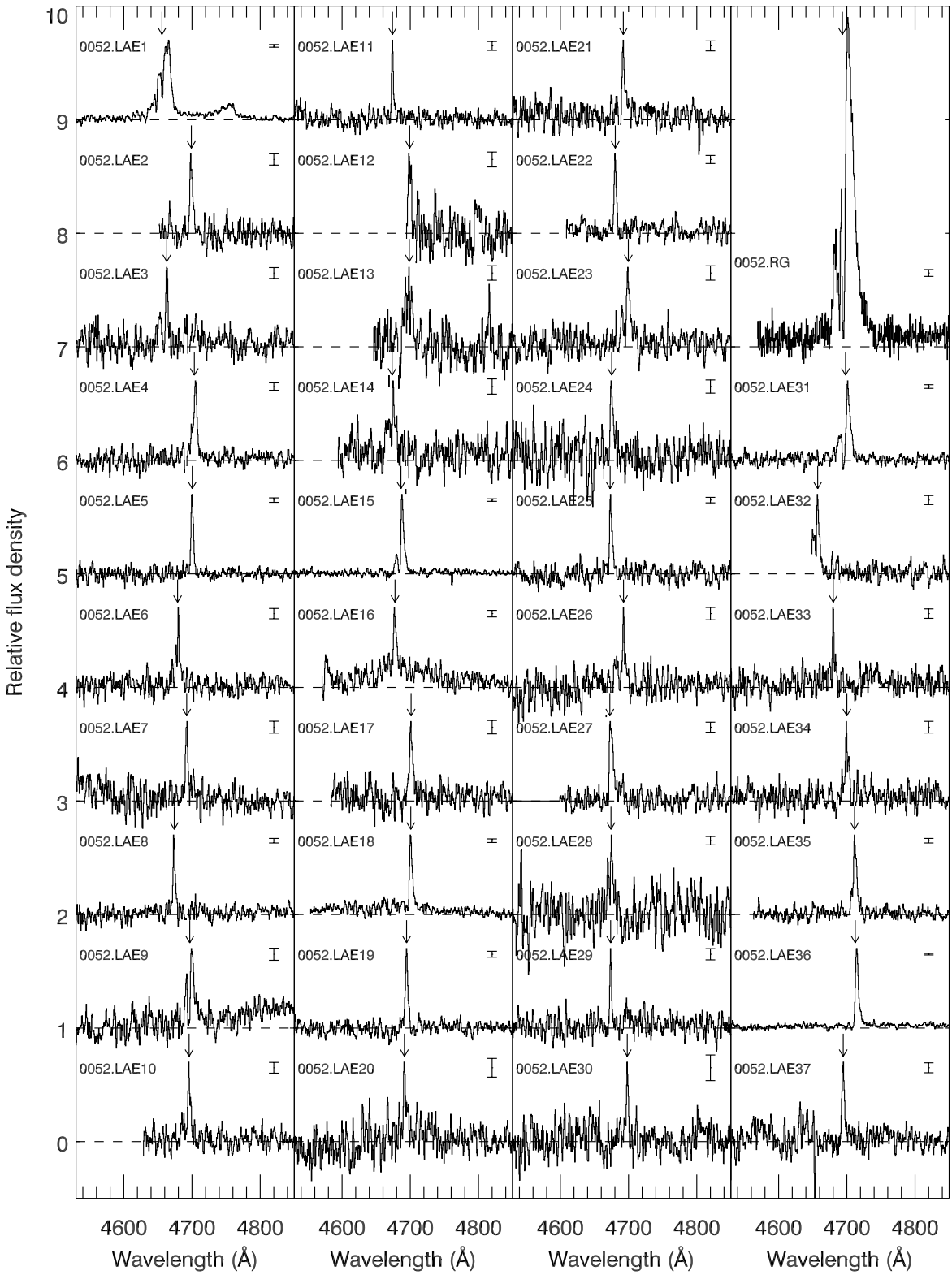

Fig. 3. Spectra of the confirmed emitters near the radio galaxy MRC 0052–241. The spectrum of the radio galaxy is shown in the top-right panel of the Figure. The error bar in the right corner of each spectrum indicates the average error in the flux density of each pixel. All spectra are boxcar averaged over three pixels and normalized to the peak of the Lyα line at a relative flux density of 0.7. The offset between the spectra is 1.0. The arrow indicates the center of the emission line of each emitter. The redshift, flux and width of the emission lines can be found in Table A.2.

3.5. MRC 0943–242, z = 2.92

This powerful radio source with a flux density of 1.1 Jy at 408 MHz has a redshift of $z = 2.923$ (Röttgering et al. 1995; Röttgering et al. 1997). The radio galaxy is surrounded by a metal-enriched, low surface brightness gas halo extending for at least 8″ (67 kpc, Villar-Martín et al. 2003). The estimated dynamical mass of the gas halo is $7{-}44 \times 10^{11}$ $M_{\odot}$

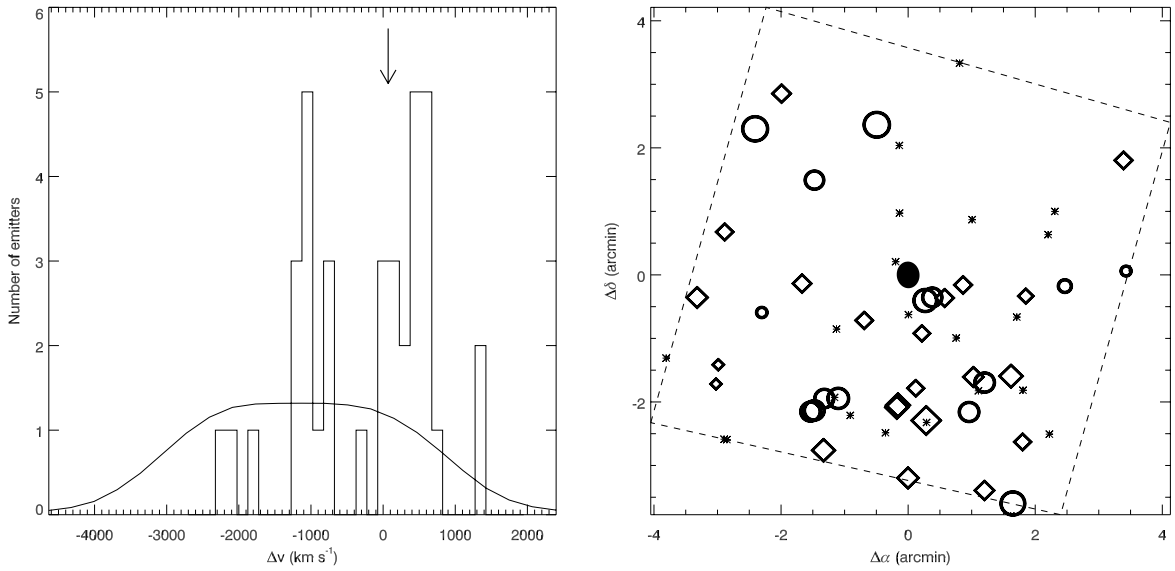

Fig. 4. *Left*: velocity distribution of the confirmed emitters near MRC 0052–241. The median redshift ($z = 2.8600$) of the emitters is taken as zero-point. The bin size is 150 km s^{-1}. The relative velocity of the radio galaxy (70 km s^{-1}, see Table A.2) is indicated by an arrow. The solid line represents the selection function of the narrow-band filter, normalized to the total number of confirmed emitters. *Right*: spatial distribution of the confirmed (circles and diamonds) and remaining candidate (stars) Lyα emitters. The dashed quadrangle represents the outline of the imaging area. The radio galaxy is denoted by a filled ellipse, that depicts the approximate shape and position angle of the radio galaxy Lyα halo (see Table 5). The circles represent the emitters with a redshift smaller than the median redshift ($z < 2.8600$) and the diamonds those with $z > 2.8600$. The size of the symbols are scaled according to the velocity offset from the median, with smaller symbols standing for emitters with a redshift farther from the median.

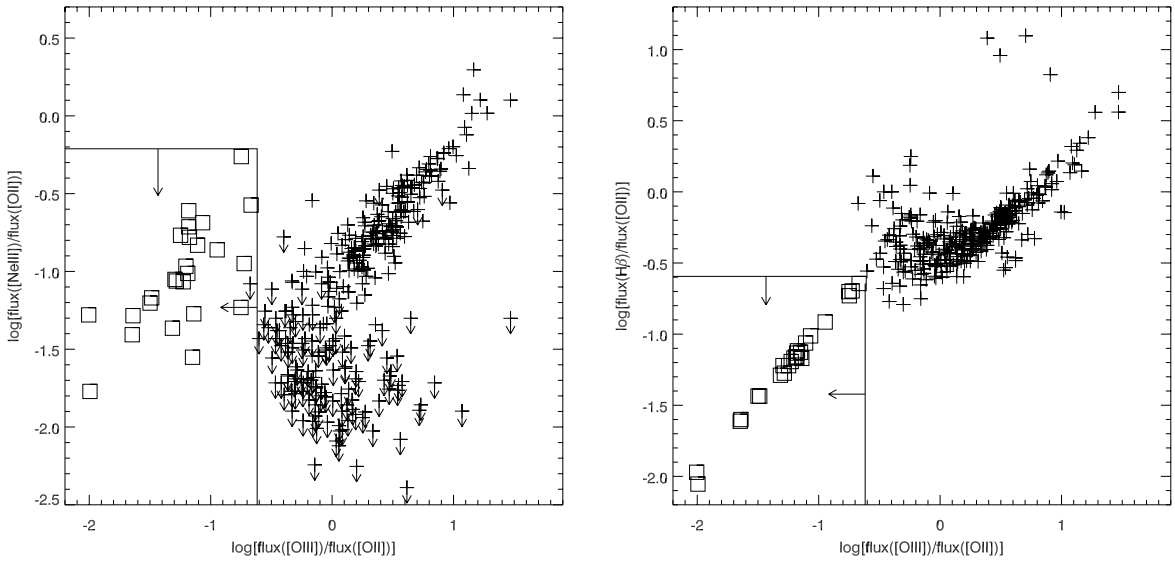

Fig. 5. Limits on the observed flux ratios for the single emission line sources near MRC 0943–242 (squares). All limits are 2σ upper limits. Line ratios of low redshift [O II] emitters from Terlevich et al. (1991) are plotted as pluses. The measured limits on the line ratios are consistent with the identification of the emission lines with Lyα (see text).

(Villar-Martín et al. 2003; Jarvis et al. 2003). This could be an indication that we are witnessing the formation of a massive galaxy.

Imaging and spectroscopic observations

The field surrounding the radio galaxy was observed with the VLT in 2001 March. Images were taken in the narrow-band for 375 min and 75 min in the *B*-band (Table 2). A part of the field (1.1 arcmin^2) was not usable to search for Lyα emitters due to the presence of a bright star (*R* magnitude of 8.7) located 2.″5 to the north-west of the radio galaxy. A total of 65 emission line candidates with $EW_0 > 15$ Å and $\Sigma > 3$ is found in the images.

Additional images of the field were taken in 2003 February and 2004 January with the LRIS instrument on the Keck I telescope. Observations were done in the u'-band (for 277 min), *V*-band (93 min) and *I*-band (100 min). The main purpose of these images is to search for Lyman-break galaxies in the field. In this paper we use the images only to separate possible Lyα emitters at $z \sim 2.9$ from low redshift line emitters.

Follow-up spectroscopy was carried out during two observing sessions with LRIS on Keck I. In total, four user-defined slitmasks were observed with exposure times between 120 and 180 min (Table 4). In the four masks, 30 of the 65 candidate Lyα emitters were observed. Of these 30 objects, 26 showed an

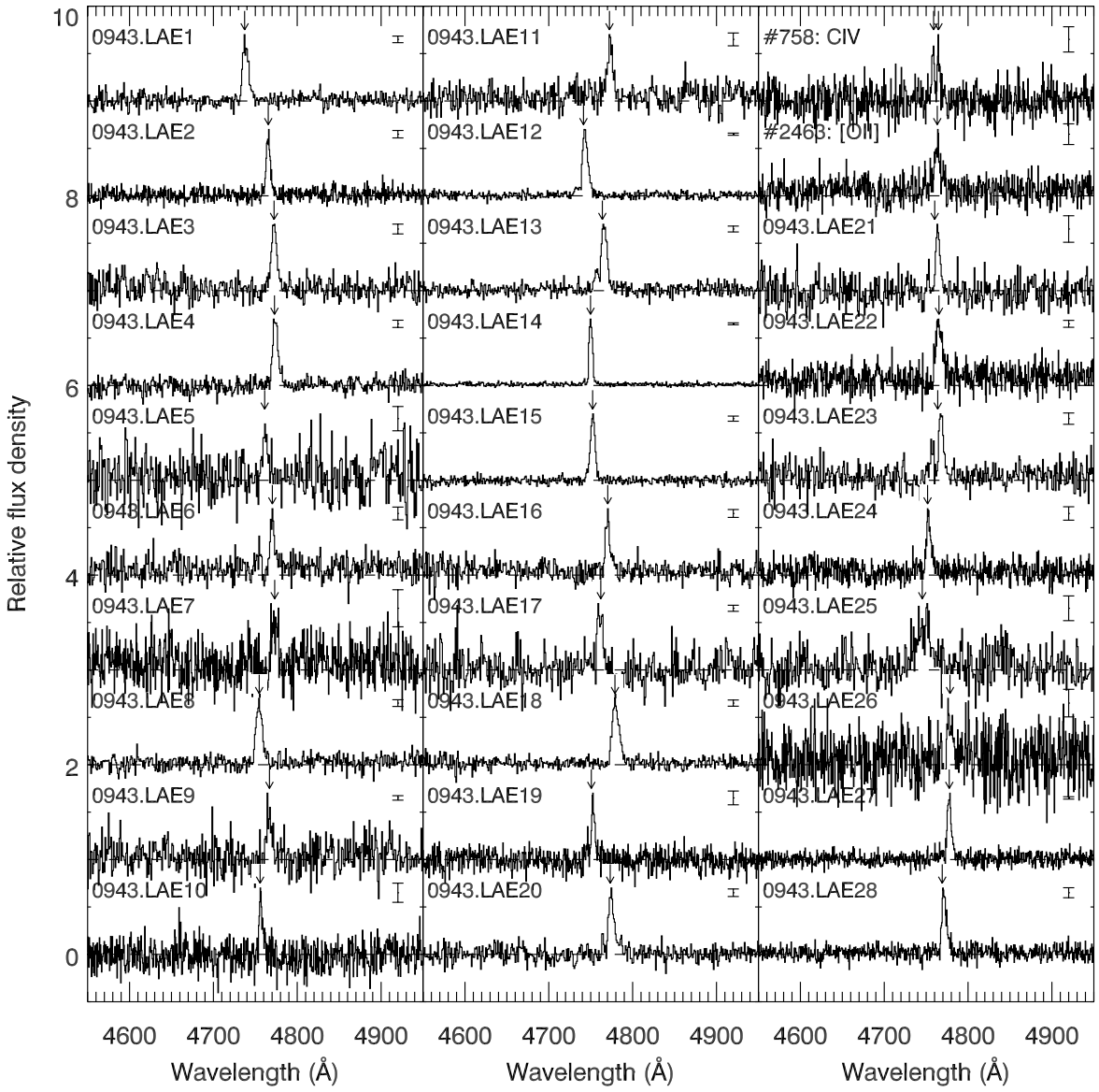

Fig. 6. Spectra of the confirmed emitters and low redshift interlopers near the radio galaxy MRC 0943–242. The average uncertainty in the flux density over the wavelength range 4550 Å $< \lambda <$ 4950 Å is plotted as an error bar in the right corner of each spectrum. All spectra are normalized to the peak of the Lyα line at a relative flux density of 0.7. The offset between the spectra is 1.0. The arrow indicates the center of the emission line of each object. The redshift, flux and width of the emission lines can be found in Table A.3.

emission line at the wavelength expected for Lyα at $z = 2.9$, the remaining four did not show a line (or continuum) in their spectrum. These four unconfirmed emitters were among the five faintest emitters observed. Most likely, the emission lines of the four objects are too faint to be detected. In addition to the 26 confirmed emission line galaxies, four objects which had a predicted Lyα equivalent width <15 Å also showed an emission line in their spectrum. The spectra of these 30 emission line objects are shown in Fig. 6.

Line identification

The next question is whether these 30 line emitters are due to Lyα at $z \simeq 2.9$. In contrast to the observations of the 0052 field, the resolution of the spectra was not high enough to resolve the [O II] doublet.

For three galaxies the redshift could be securely derived. One of these objects (# 758 in Fig. 6) is identified as a C IV $\lambda\lambda$1548, 1551 emitter at $z = 2.07$ as its emission line is resolved into two lines separated by ~8 Å. The redshifts of two other objects are confirmed by the presence of other emission lines in their spectrum. In the spectrum of emitter 0943.LAE25 N V λ1240 is detected, confirming that the object is a Lyα emitter at $z \sim 2.90$. The redshift of emitter 0943.LAE18 ($z \sim 2.93$) is confirmed by the detection of C IV λ1549 (and a very weak detection of He II λ1640). The relatively small *FWHM* of the Lyα line (*FWHM* = 700 km s^{-1}) suggests that this object is a type-II AGN (e.g., Norman et al. 2002).

The remaining 27 sources merely show a single emission line in their spectra, which typically cover a wavelength range of over 5500 Å. The most common and brightest low redshift emission line galaxies contaminating searches of $z \sim 3$ Lyα emitters are [O II] $\lambda\lambda$3726, 3729 emitters (e.g., Fynbo et al. 2003). To distinguish high redshift Lyα emitters from low redshift emission line galaxies, various tests can be applied (see Stern et al. 2000, for a detailed review). Below we will briefly describe and apply three tests (the asymmetry of the emission line, the

presence of a continuum break and the limits on accompanying emission lines) that are frequently used in the literature to discriminate Lyα emitters from low redshift galaxies (e.g., Stern et al. 2000; Fynbo et al. 2001; Rhoads et al. 2003; Dawson et al. 2004; Venemans et al. 2004).

• *Emission line asymmetry.* This test, which makes use of the characteristic blue wing absorption profile of the Lyα emission line, has been successfully applied to confirm $z > 4.5$ Lyα emitters (e.g., Kodaira et al. 2003; Rhoads et al. 2003; Dawson et al. 2004; Hu et al. 2004). What makes this test extra useful is that a blended [O II] doublet would appear as a single line with *excess* emission on the blue side, because the redder line of the doublet is stronger in star forming galaxies (Rhoads et al. 2003). To quantify the asymmetry of an emission line, Rhoads et al. (2003) introduced the two asymmetry parameters a_λ ("wavelength ratio") and a_f ("flux ratio"). These parameters depend on the wavelength where the flux peaks (λ_p), and where the flux is at 10% of the peak value on the red side ($\lambda_{10,\mathrm{r}}$) and the blue side ($\lambda_{10,\mathrm{b}}$) of the emission line. Using these wavelengths, the "wavelength ratio" is defined as $a_\lambda = (\lambda_{10,\mathrm{r}} - \lambda_\mathrm{p})/(\lambda_\mathrm{p} - \lambda_{10,\mathrm{b}})$ and the "flux ratio" as $a_\mathrm{f} = \int_{\lambda_\mathrm{p}}^{\lambda_{10,\mathrm{r}}} f_\lambda \mathrm{d}\lambda / \int_{\lambda_{10,\mathrm{b}}}^{\lambda_\mathrm{p}} f_\lambda \mathrm{d}\lambda$ (Rhoads et al. 2003, 2004; Dawson et al. 2004). Dawson et al. (2004) found that $z = 4.5$ Lyα emitters have $a_\lambda > 1.0$ and/or $a_\mathrm{f} > 1.0$, while [O II] emitters at $z \sim 1$ typically have $a_\lambda \approx 0.8$ and $a_\mathrm{f} \approx 0.8$.

However, this line asymmetry test critically depends on the assumption that a large fraction of the blue part of the Lyα emission line is absorbed by neutral hydrogen. Although absorption is often present, there can still be a significant amount of flux on the blue wing (see the emission lines in e.g. Fig. 3, Tapken et al. 2004, V05). Also, due to the absorption the peak of the Lyα line could move to the red, reducing the flux that appears to be redward of the peak (see e.g. the spectra on the left side of Fig. 9 and the spectra in V05). As a consequence, the asymmetry parameters for a Lyα line can be smaller than 1.0. For example, if the spectrum of the radio galaxy MRC 0943−242 would be convolved with a Gaussian with a $FWHM \approx 250$ km s^{-1} (or would be observed with slightly lower resolution), then the asymmetry parameters would give $a_l = 0.67$ and $a_\mathrm{f} = 0.92$. Also, the asymmetry parameters of emitter 0052.LAE1, which is a QSO at $z = 2.86$ as confirmed by N V, are $a_l = 0.48$ and $a_\mathrm{f} = 0.38$ and those of emitter 0052.LAE31 measure $a_\lambda = 1.0$ and $a_\mathrm{f} = 0.41$. Thus, while lines with $a_\lambda > 1.0$ or $a_\mathrm{f} > 1.0$ are most likely Lyα lines, a profile with low values of a_λ and a_f could be either an [O II] or a Lyα line.

With this caveat in mind, we measured the asymmetry of our single emission line sources. 21 have $a_\lambda > 1.0$ and/or $a_\mathrm{f} > 1.0$, and these emission lines are most likely Lyα lines at $z \simeq 2.9$. The identification of the remaining six lines remains problematic and we have to rely on others tests to secure the redshift.

• *Continuum break.* A prominent feature of high redshift galaxies is the absorption of the continuum blueward of the Lyα line, caused by neutral hydrogen located in the galaxy between the galaxy and the observer (e.g., Madau 1995). To measure whether the continuum of the line emitters has a discontinuity, we looked at the u'- and V-band images. For a galaxy at $z = 2.9$ the central wavelength of the u' filter lies below the 912 Å Lyman limit, while the V-band begins just redward of the Lyα line. Based on a large imaging and spectroscopic survey of high redshift galaxies, Cooke et al. (2005) estimate that the vast majority of galaxies at $z \sim 3$ have a break of $u' - V > 1.2$−1.6. On the other hand, low redshift objects with the Balmer/4000 Å break that falls between the u'- and V-band have a color of $u' - V \ll 1.5$ (e.g., Hammer et al. 1997).

Of the 27 single emission line sources, 26 were inside the field of view of the u'-band image. Two objects were too close to a bright foreground object to reliably measure the magnitude. Of the remaining 24 sources two are detected in the u'-band, the others are not detected. The undetected emitters have typically 2σ limits of $m_{u'} > 27.6$ within an aperture radius of 1.″2, which is twice the radius of the seeing disc. One of the two detected objects in the u'-band has a signal-to-noise of ∼2.0 and a $u' - V \simeq 2.5$ is measured for this object. The second detection, of emitter # 2463 in Fig. 6, has a signal-to-noise of 8 and a $u' - V = 1.0$. Combined with a measured line asymmetry of $a_\lambda = 0.7$ and $a_\mathrm{f} = 0.7$, we conclude that this emitter is a foreground galaxy. The emission line can be most likely identified with [O II] at a redshift of $z \sim 0.28$. It should be noted that this source had a predicted equivalent width of 9 Å, and was therefore not in our list of priority candidate Lyα emitters.

Five out of 24 emission line objects have large breaks with a 2σ limit of $u' - V > 2.0$. These objects can securely be identified with high redshift Lyα emitting galaxies. For the remaining 18 emission line galaxies, either the continuum was too faint to detect a large $u' - V$ break in our images or the photometry in the V-band was unreliable due to the presence of a nearby bright object.

• *Emission line intensity ratios.* Although no other emission lines were found in the spectra of the 27 emission line sources, we can derive upper limits on various line ratios. This is very useful because several other emission lines are expected in the typical spectrum of an [O II] emission line galaxy, such as [Ne III]λ3869, Hβ and [O III]λ5007.

What makes this test very useful to us, is the large wavelength range of the spectra of the emission line sources. If the emission line in the spectrum is [O II], then we are able to place limits on the flux of the [Ne III]λ3869, Hβ and [O III]λ5007 lines. Although Hα is also within the probed wavelength range, it falls in a region where bright skylines dominate the spectrum, and the Hα upper limits are not useful. Instead, we measured the limits on the expected positions of [Ne III], Hβ and [O III]. Two sigma limits were computed in a region which is twice the *FWHM* of the detected emission line. The limits on various emission line ratios are presented in Fig. 5. To compare our limits with low redshift [O II] emitters, we also plotted line ratios as found by Terlevich et al. (1991) for local H II galaxies. In all cases, our observed ratios lie in a region outside the values found for local galaxies with [O II] in emission. We therefore conclude that the emission line objects are Lyα emitters.

To summarize, after applying three tests that can discriminate Lyα emitters from low redshift emission line galaxies, we have identified one [O II] emitter (object #2463 in Fig. 6) and confirm that the remaining 26 Lyα emitters are at $z \sim 2.9$. Combined with the two emitters with C IV in their spectrum, the total number of Lyα emitters near the radio galaxy MRC 0943−242 is 28. The properties of the Lyα emission lines of these $z = 2.9$ galaxies are printed in Table A.3.

A large scale structure of Lyα emitters

The volume densities of emitters near MRC 0943–242 and near the radio galaxy MRC 0316–257 (V05) are very similar. Down to a narrow-band magnitude of $m_\mathrm{nb} = 26.1$ there are 63 emitters in the 0943 field compared to 59 in the 0316 field. Correcting for the difference in observed comoving volume, the density ratio is $n_{0943}/n_{0316} = 1.0^{+0.2}_{-0.2}$. This translates to a density of $n_{0943} = 3.2^{+0.9}_{-0.7}$ times the field density. Comparing directly to blank field surveys for $z \sim 3$ Lyα emitters gives similar results (see also Sect. 3.4). For example, the field density of

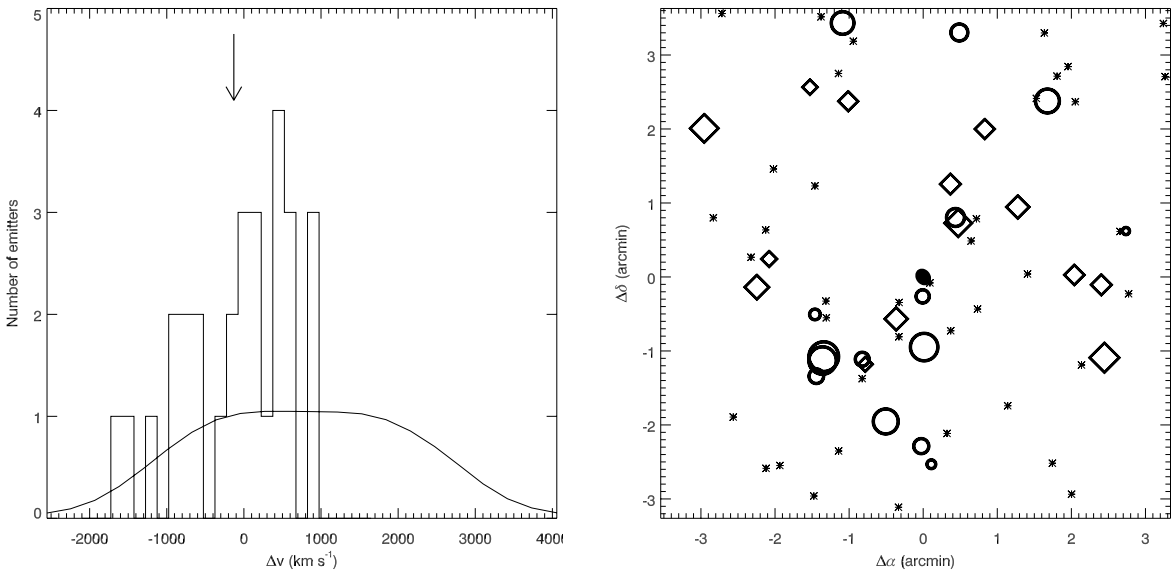

Fig. 7. Same as Fig. 4, but for the velocity distribution (*left*, the median redshift of the emitters ($z = 2.9201$) is used as zeropoint) and spatial distribution (*right*) of the emitters near MRC 0943–242.

Lyα emitters at $z \simeq 3.1$ was measured by Hayashino et al. (2004) in the 0.17 deg^2 Subaru Deep Field. They estimate a space density of $n_{\rm field} = 3.5 \times 10^{-4}$ Mpc^{-3} for Lyα emitters with a rest frame equivalent width >37 Å down to a narrow-band magnitude of 25.3. Applying the same selection criteria (taking into account the difference in luminosity distance) gives a space density of emitters in the field of MRC 0943−242 of $n_{0943} = 9.6 \times 10^{-4}$ Mpc^{-3}. The density ratio is $n_{0943}/n_{\rm field} = 2.7^{+1.3}_{-0.9}$. When compared to the space density of Lyα emitters found by Ciardullo et al. (2002), the overdensity in the 0943 field is $n_{0943}/n_{\rm field} = 5.2^{+2.7}_{-1.8}$. All three estimates of the density presented here are consistent with each other. The weighted average of the estimates is $3.4^{+0.8}_{-0.6}$.

In Fig. 7 the velocity and spatial distribution of the emitters is shown. Although the emitters have no preferred position on the sky, they are clustered in velocity space. We can estimate the significance of the clustering by performing Monte Carlo simulations of the redshift distribution. We reproduced 10 000 realizations of 28 emitters using the narrow-band filter curve as redshift probability function for each emitter. We find that both the mean velocity and the dispersion of the emitters are significantly smaller than that of the simulated redshift distributions at a level of $\sim 3.3\sigma$ (Fig. 8)[3]. This is a strong indication that the suggested grouping of Lyα emitters is not a projection effect. The velocity dispersion of the confirmed emitters is 715 ± 105 km s^{-1}. This dispersion could be a lower limit, since no clear edge is visible in the distribution on the negative velocities side.

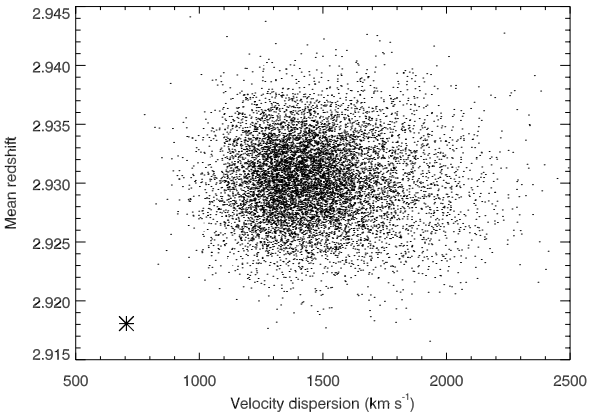

Fig. 8. Velocity dispersion (σ_v) and mean redshift ($\bar{z}$) of 10 000 simulated redshift distributions of 28 emitters. In these simulations, the narrowband filter curve was used as redshift probability function. The simulated distributions have a mean redshift of $\bar{z} = 2.930 \pm 0.004$ and a velocity dispersion of $\sigma_v = 1475 \pm 235$ km s^{-1} (the errors represent the standard deviations between the simulations). These simulated values are significantly different (at the 4.7σ level) compared with the observed velocity dispersion and mean redshift of the emitters near MRC 0943–242 of $\sigma_v = 715$ km s^{-1} and $\bar{z} = 2.918$ (indicated with a cross).

3.6. MRC 0316–257, z = 3.13

This 1.5 Jy radio source from the Molonglo Reference Catalogue (Large et al. 1981) lies at a redshift of 3.13 by McCarthy et al. (1990). This target was especially interesting, because Le Fèvre et al. (1996) found two bright Lyα emitters close to the radio galaxy, which indicated that this radio galaxy is in an overdense environment. Narrow- and broad-band imaging of this field with the VLT resulted in the discovery of 77 candidate Lyα emitters. Follow-up spectroscopy revealed 33 emission line galaxies of which 31 are Lyα emitters near the radio galaxy, while the remaining two are foreground galaxies. By comparing the number density of Lyα emitters near the radio galaxy to that of the field, the overdensity of emitters near 0316 is estimated to be a factor $3.3^{+0.5}_{-0.4}$ times the field density (V05). The velocity distribution of the emitters has a width of $FWHM = 1510$ km s^{-1}, which is smaller than the width of the narrow-band filter ($FWHM \sim 3500$ km s^{-1}). The peak of the distribution is located within 200 km s^{-1} of the redshift of the radio galaxy. In V05 we have shown that the confirmed emitters are members of a protocluster at $z \sim 3.13$ with an estimated mass of $>3 \times 10^{14}\ M_\odot$.

[3] Recently, Monaco et al. (2005) investigated the effect of peculiar velocities on the redshift distribution of Lyα emitters using dark matter simulations. They found that the velocity dispersion of Lyα emitters is smaller than based on the Monte Carlo simulations described above, lowering the significance of the redshift clumping.

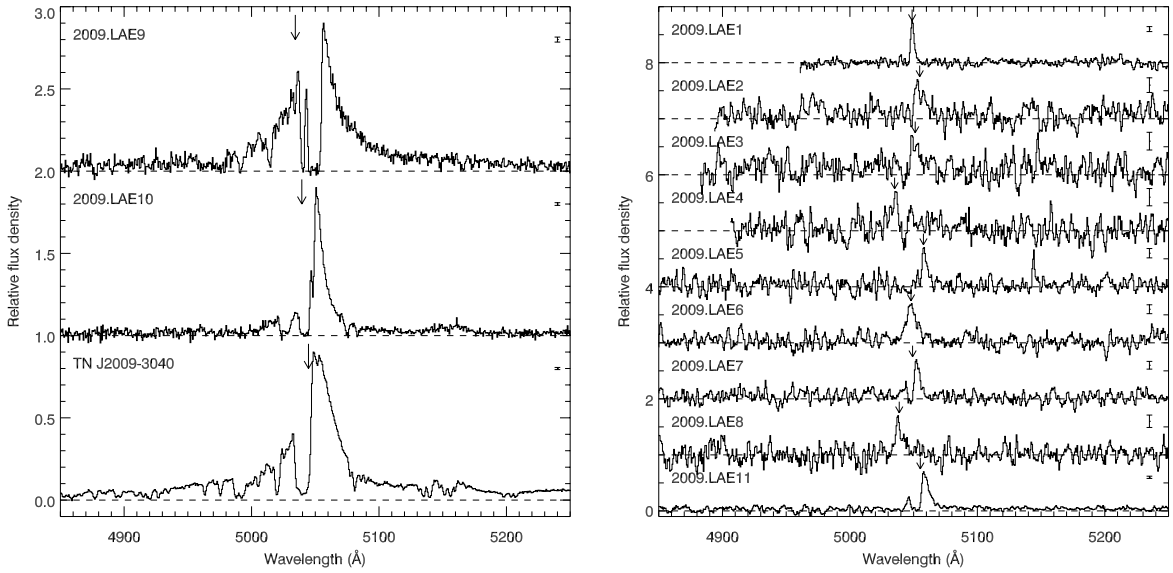

Fig. 9. Spectra of the confirmed emitters near the radio source TN J2009–3040. The spectra of the radio source and two quasars companions are shown on the left, and on the right the confirmed Lyα emitters are plotted. The spectra in the *right panel* are boxcar average over three pixels. The uncertainty per pixel is shown as error bar on the right of each spectrum. The arrow indicates the central wavelength of the emission line. The redshift, flux and width of the emission lines can be found in Table A.4.

3.7. TN J2009–3040, z = 3.15

This radio source was selected by De Breuck et al. (2000) as an ultra steep spectrum radio source ($\alpha = -1.36$, with $f_\nu \propto \nu^\alpha$) and was identified with a $m_K = 18.05 \pm 0.05$ object which has a strong unresolved component (De Breuck et al. 2002). Spectroscopy of this object revealed three emission lines, including Lyα with a *FWHM* of ∼2000 km s^{-1} at a redshift of 3.156. Based on the width of the emission lines and the morphology of the source, this radio source is identified as a quasar (C. De Breuck, private communications).

Imaging observations

Obtaining deep images of this field was challenging for two reasons. First, the field is located close to the galactic centre ($l = 11°$ and $b = -30°$) and the extinction towards the radio source is high, with an $E(B-V) = 0.181$ (Schlegel et al. 1998). Secondly, due to emission from inside our Galaxy the background towards the quasar is not flat, but varies up to 10% over scales of roughly 10″. We removed this variable background by subtracting the median pixel value calculated in 10″ × 10″ boxes surrounding each pixel.

Spectroscopic observations and results

Analysis of the narrow-band and V-band images resulted in a list of 21 candidate Lyα emitters. In 2002 September spectra were taken of nine of these candidates for 330 min with FORS2. The use of the 1400V grism (with a resolution of $R = 2100$) allowed us to identify low redshift interlopers like [O II] emitters (see Fig. 2), similar to the 0052 field. We confirmed that all nine candidates were Lyα emitters at $z \sim 3.15$ (Fig. 9). Two objects with predicted $EW_0 \simeq 10$ Å and $\Sigma \simeq 2.5$ (2009.LAE2 and 2009.LAE5 in Fig. 9 and Table A.4) were also confirmed to be Lyα emitters near the radio source. Two galaxies with a predicted $EW_0 \simeq 6$ and 9 Å were confirmed to be [O II] emitters at $z \sim 0.35$ (bottom two spectra in Fig. 2). In total, 11 Lyα emitters are found near the radio source. Two of these emitters are broad-line QSOs with a *FWHM* of 1600 and 3200 km s^{-1} (see left panel of Fig. 9).

The detection of (broad-line) QSOs near radio galaxies is quite common. In each of the radio galaxy fields described in this paper, at least one of the Lyα emitters is confirmed to have a line *FWHM* of >1000 km s^{-1} (see Tables A.1−A.5), an indication that these objects harbour an active galactic nucleus (AGN). In the protocluster near the radio galaxy MRC 1138−262 at $z = 2.16$ (Sect. 3.3) at least four QSOs are confirmed (Pentericci et al. 2002; Croft et al. 2005).

In Fig. 10 the velocity histogram and the spatial distribution of the confirmed Lyα emitters are shown. The median redshift of the emitters lies 170 km s^{-1} away from the radio source. The velocity dispersion of the emitters as calculated with the Gapper scale estimator (which is preferred for low ($n \simeq 10$) number statistics, Beers et al. 1990) is 515 ± 85 km s^{-1}. This is a factor ∼3 smaller than that of the narrow-band filter, which has a $\sigma = 1490$ km s^{-1}. Monte Carlo simulations of the distribution of 11 emitters through the narrow-band filter, we found that there is an 8% chance that the velocities of the emitters are drawn from a random distribution. On the sky, the emitters appear to be concentrated on the southern half of the field. The position of the radio source is on the edge of the distribution of Lyα emitters, very similar to the situation in the field of TN J1338−1942 at $z = 4.1$ (Venemans et al. 2002, Sect. 3.8).

Volume density

We can compare the number density of Lyα emitters in this field directly to that of the 0316 field, because the same narrow-band filter was used. The number of (candidate) emitters down to the same luminosity limit is in the 2009 field a factor $2.0^{+0.7}_{-0.5}$ smaller than that in the 0316 field. The 0316 field is overdense by a factor $3.3^{+0.5}_{-0.4}$ (V05), which implies that the number density of Lyα emitters near TN J2009−3040 is a factor $1.7^{+0.8}_{-0.6}$ times the field density, with is consistent with no overdensity. However, nine out of 11 confirmed emitters lie south of the radio galaxy, as do nine out of 12 unconfirmed candidates (Fig. 10). This could indicate that (locally) the volume density of Lyα emitters near the radio source TN J2009−3040 is much higher than the field density. Although the volume density of Lyα emitters near

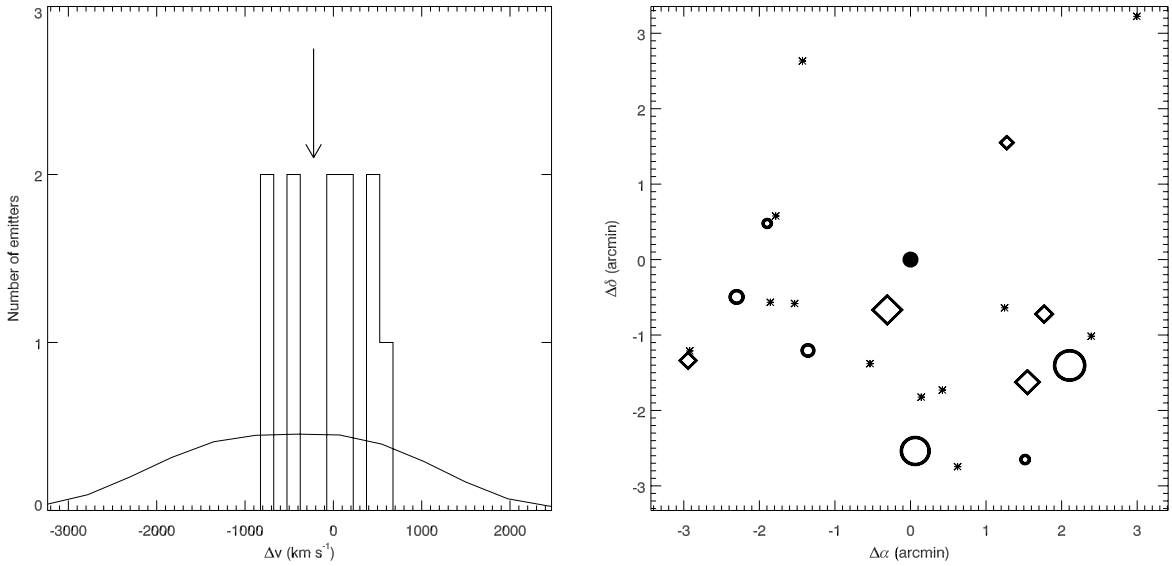

Fig. 10. Same as Fig. 4, but for the velocity distribution (*left*, the median redshift of the emitters ($z = 3.1528$) is used as zeropoint) and spatial distribution (*right*) of the emitters near TN J2009−3040.

TN J2009−3040 is consistent with the field density at that redshift, the clustering both on the sky and in velocity space of the emitters could points to a structure of galaxies. More observations are needed to determine the reality of this clustering.

3.8. TN J1338−1942, z = 4.11

This radio galaxy has a redshift of 4.1 (De Breuck et al. 1999, 2001) and is one of the brightest known in Lyα (De Breuck et al. 1999, 2001). Because no narrow-band filter is available at the VLT that is centred on the wavelength of a Lyα line at $z = 4.1$, we used a custom narrow-band filter with an effective wavelength of 6199 Å and a *FWHM* of 59 Å. Narrow-band and *R*-band imaging and follow-up spectroscopy with the VLT of the field of TN J1338−1942 revealed 20 Lyα emitters within a projected distance of 1.3 Mpc and 600 km s^{-1} of the radio galaxy (Venemans et al. 2002). The structure is overdense in Lyα emitters by a factor of 4−15 and could be the ancestor of a rich cluster of galaxies. Multi-color imaging with the Advanced Camera for Surveys (ACS) on board the *Hubble Space Telescope (HST)* revealed an anomalously large number of LBGs near the radio galaxy, confirming the presence of a protocluster at $z = 4.1$ (Miley et al. 2004; Overzier et al. 2006a).

New observations

The VLT observations presented in Venemans et al. (2002) showed that the emitters are not distributed homogeneously over the field, but appear to have a boundary in the north-west. To further determine the extent and shape of the protocluster region, the field near TN J1338−1942 was imaged at a second position. The second pointing is located towards the south-east of the radio galaxy and overlaps the first field (hereafter the 1338-1 field) at the position where the concentration of Lyα emitters seemed to be the highest (see Fig. 11 for the outline of the imaging areas). The second field (hereafter 1338-2) was observed for 420 min in the narrow-band and for 75 min in the *R*-band. Analysis of data in the second field resulted in the discovery of 35 candidate emitters. Ten candidate emitters were also selected as candidates in the 1338-1 field and eight of them were confirmed by Venemans et al. (2002). One candidate emitter in the second field catalogue has an $EW_0 = 19^{+14}_{-5}$ Å, but a computed equivalent width of 9^{+6}_{-3} Å in the first field catalogue. The (weighted) average of these two measurements is $EW_0 \simeq 14.5$ Å. Because this is below our selection criterion of $EW_0 = 15$ Å, we removed the object from our candidate list. Follow-up spectroscopy showed that the object is an [O II] emitter at $z \sim 0.66$. The total number of candidate emitters in the two fields combined is 54.

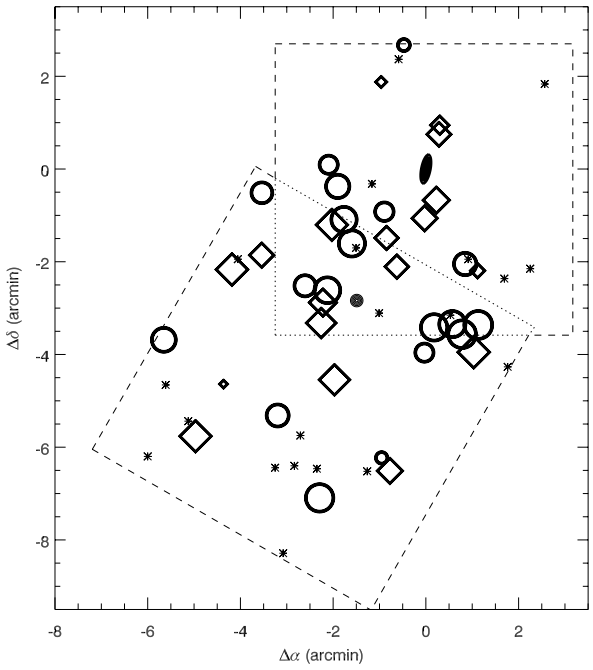

Fig. 11. Spatial distribution of the confirmed and candidate Lyα emitters near TN J1338–1942. Symbols and their sizes are the same as in Fig. 4. The filled circle at (−1.′5, −2.′8) represents the centre of all the emitters. The dashed lines outline the area covered by the VLT images.

Spectroscopic observations of candidate emitters in the second field were carried out in 2003 February with Keck/LRIS (150 min) and in 2003 March with VLT/FORS2 (310 min,

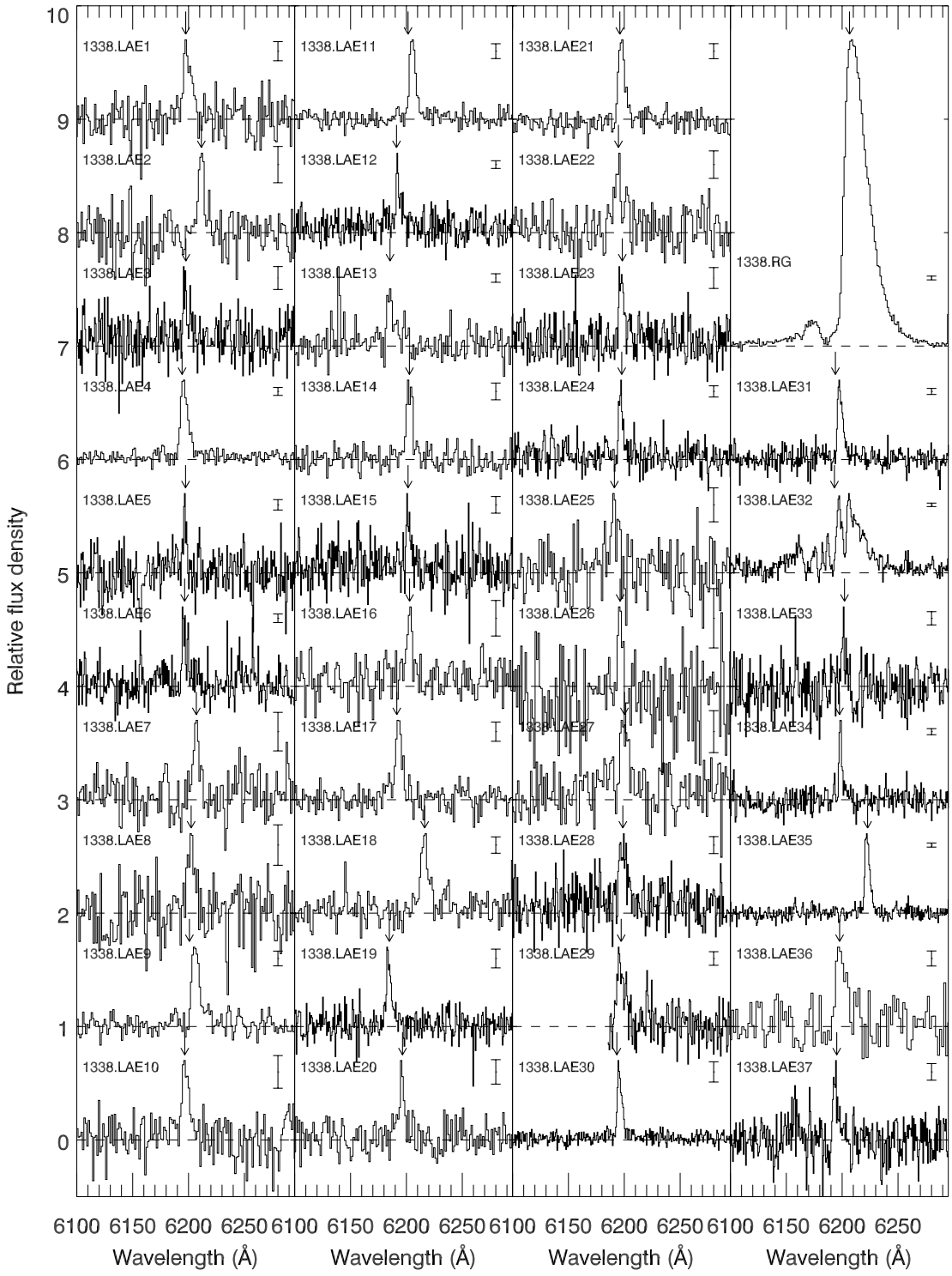

Fig. 12. Spectra of the confirmed emitters near the radio galaxy TN J1338–1942. Error bars (right in each panel) represent the uncertainties in the flux density average over all pixels in the plotted wavelength range. All spectra are normalized to the peak of the Lyα line, which has a relative flux density of 0.7. The offset between the spectra is 1.0. The arrow indicates the central wavelength of the Lyα emission line. The redshift, flux and width of the emission lines can be found in Table A.5.

see Table 4). In the two observing sessions combined, spectra were taken of 15 good candidate emitters. In addition, objects were observed that were lower on our priority list. These additional objects included four emitters that were already confirmed by Venemans et al. (2002), six candidate emitters with 9 Å $< EW_0 <$ 15 Å and five galaxies with an $EW_0 >$ 15 Å, but with a signal-to-noise in the narrow-band image of ∼4.

Of the 15 good candidate emitters, 13 were confirmed to be Lyα emitters at $z \sim 4.1$. The two unconfirmed emitters were among the faintest candidates that were observed in that mask. From the additional objects that were observed, the four emitters that were confirmed by Venemans et al. (2002) were all reconfirmed. Among the low equivalent width sources was one Lyα emitter at $z = 4.1$ and five [O II] emitters at a

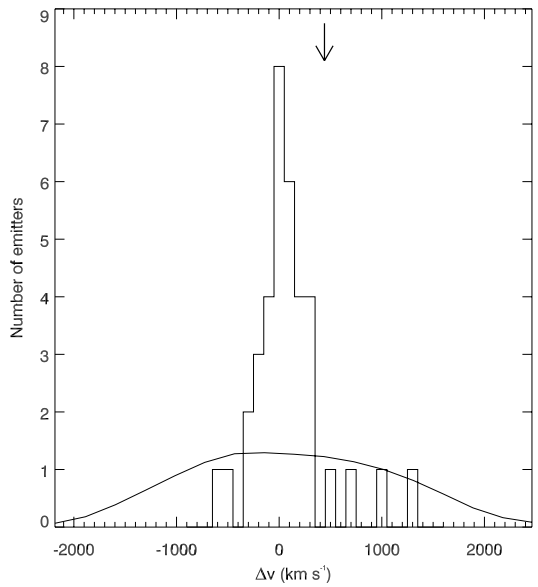

Fig. 13. Velocity distribution of the confirmed emitters near TN J1338–1942. The median of the emitters ($z = 4.0977$) is taken as zero-point. The velocity of the radio galaxy ($\Delta v = 440$ km s^{-1}) is indicated by an arrow. The solid line represents the selection function of the narrow-band filter, normalized to the total number of confirmed emitters.

redshift $z \simeq 0.66$. The low signal-to-noise sources added another two Lyα emitters at $z = 4.1$ to the list of confirmed emitters. Combined with the data described in Venemans et al. (2002), the total number of confirmed Lyα emitters at $z \sim 4.1$ is 37. In Fig. 12 the spectra of the confirmed emitters and of the radio galaxy are shown. In Table A.5 the properties of the emission lines are listed.

Volume density

Several blank field surveys for Lyα emitters at redshifts between $z = 4$ and $z = 5$ have been conducted in recent years. The two surveys covering the largest area are the LALA survey, aimed at finding Lyα emitters at $z = 4.5$ (Rhoads et al. 2000; Dawson et al. 2004), and the Subaru Deep Field (SDF) survey, in which was searched for Lyα emitters at $z = 4.8$ (Ouchi et al. 2003; Shimasaku et al. 2003, 2004).

To estimate the (over)density of Lyα emitters near TN J1338–1942, we compare our density to that found in the LALA and SDF surveys. The LALA survey probed a volume of 1.5×10^6 comoving Mpc^3 and ∼350 candidate Lyα emitters were discovered in this volume with an observed equivalent width >80 Å and a 5σ line flux $>2 \times 10^{-17}$ erg s^{-1} cm^{-2} (Rhoads et al. 2000; Dawson et al. 2004). Follow-up spectroscopy confirmed 72% of the targeted sources (Dawson et al. 2004), but we will conservatively assume that all 350 LALA candidates are genuine Lyα emitters. Applying the same luminosity and equivalent width criteria used in the LALA survey to our data selects 14 candidate Lyα emitters in our field of which 13 are confirmed (one has not been observed spectroscopically yet). Compared to the LALA survey, the density of Lyα emitters near TN J1338–1942 is a factor $5.2^{+1.8}_{-1.4}$ higher. The large errors are due to small number statistics.

The SDF survey covers an area of $25' \times 45'$, which is observed in two 1% narrow-band filters, one centred on Lyα at $z \approx 4.79$ and one at $z \approx 4.86$. The volume density of emitters with magnitudes $m_{\rm nb} < 25.5$ at these two redshifts is very similar ($2.7 \pm 0.4 \times 10^{-4}$ Mpc^{-3} at $z \sim 4.79$ and $3.1 \pm 0.5 \times 10^{-4}$ Mpc^{-3} at $z \sim 4.86$, Shimasaku et al. 2004). Selecting Lyα emitters in our field in the same way as was done in the SDF by Shimasaku et al. (2003), and comparing our numbers to those at $z = 4.79$ and $z = 4.86$ gives an overdensity of $4.5^{+1.3}_{-0.9}$. The weighted average of these density measurements is $n_{1338}/n_{\rm field} = 4.8^{+1.1}_{-0.8}$, consistent with the overdensity found by Venemans et al. (2002).

Structure properties

As mentioned in Venemans et al. (2002), the spatial distribution of emitters near 1338 is not homogeneous over the field. In Fig. 11 the spatial distribution is plotted of all the confirmed and candidate emitters in the two fields. The average position of the emitters (filled circle in Fig. 11) lies approximately 1.′5 east and 2.′8 south of the radio galaxy. The radio galaxy appears to be at the (northern) edge of the galaxy distribution. In contrast to the position on the sky of the Lyα emitters, De Breuck et al. (2004) found an overdensity of mm galaxies just *north* of the radio galaxy in this field. Although there is no spectroscopic confirmed whether the mm galaxies belong to a structure at the redshift of the radio galaxy, it is possible that different galaxy populations in the protocluster have different spatial distributions (see also Sect. 5.1).

The redshift distribution of the emitters is shown in Fig. 13. The velocity distribution is very narrow, with a dispersion of only 260 ± 65 km s^{-1} (*FWHM* $= 625 \pm 150$ km s^{-1}). This is much narrower than the width of the narrow-band filter, which has a *FWHM* of 2860 km s^{-1}. Monte-Carlo simulations indicate that the chance that such a narrow redshift distribution is drawn from a random sample is only 0.05%. Although the number of confirmed emitters has almost doubled since the discovery of this protocluster, the velocity dispersion has not changed. This indicates that the confirmed emitters in both the southern and northern field are members of one single structure. The small value of the velocity dispersion might suggest that we are looking at a flattened structure like a filament perpendicular to the line of sight. However, as we will show in Sect. 5.3, the velocity dispersion of the emitters in this field is in line with predictions of numerical models of the formation of massive structures. The properties of this protocluster at $z = 4.1$ will be described in more detail in Sect. 5.

3.9. TN J0924–2201, z = 5.20

TN J0924–2201 is currently the highest redshift radio galaxy known with a redshift of $z = 5.2$ (van Breugel et al. 1999). To select Lyα emitters in this field, a custom narrow-band filter encompassing the wavelength of the Lyα line of the radio galaxy at 7537 Å was purchased. The details of the observations and candidate selection in this field are presented in Venemans et al. (2004). Follow-up spectroscopy of eight of 14 candidate Lyα emitters resulted in the discovery of six Lyα emitters near the radio galaxy (Venemans et al. 2004). The field is overdense in Lyα emitters by a factor of 1.5−6.2 times the field density at that redshift and comparable in density to the radio galaxy fields 1138, 0316 and 1338 at $z = 2.2, 3.1$ and 4.1 respectively.

3.10. Radio galaxy Lyα halos

Besides allowing the detection of candidate companion galaxies, the deep narrowband Lyα images of the radio galaxy fields also provide deep maps of the diffuse emission line halos that surround the radio galaxies. In each of the observed fields, the radio galaxy is the brightest emitter of Lyα emission, with line

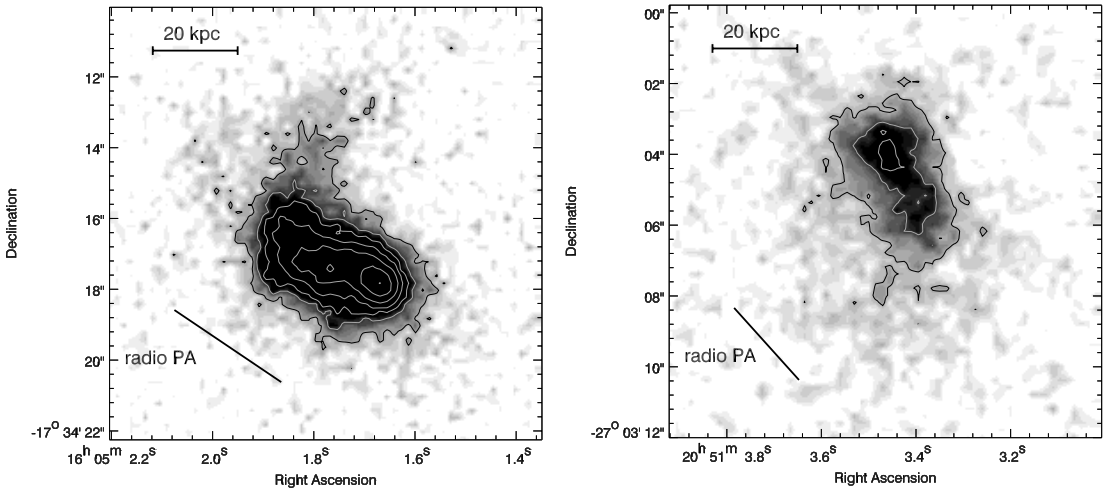

Fig. 14. Continuum subtracted Lyα halos of the radio galaxies BRL 1602–174 (*left*) and MRC 2048–272 (*right*). The depth of the images is given in Table 2. The position angle of the radio emission is indicated on the left of each plot.

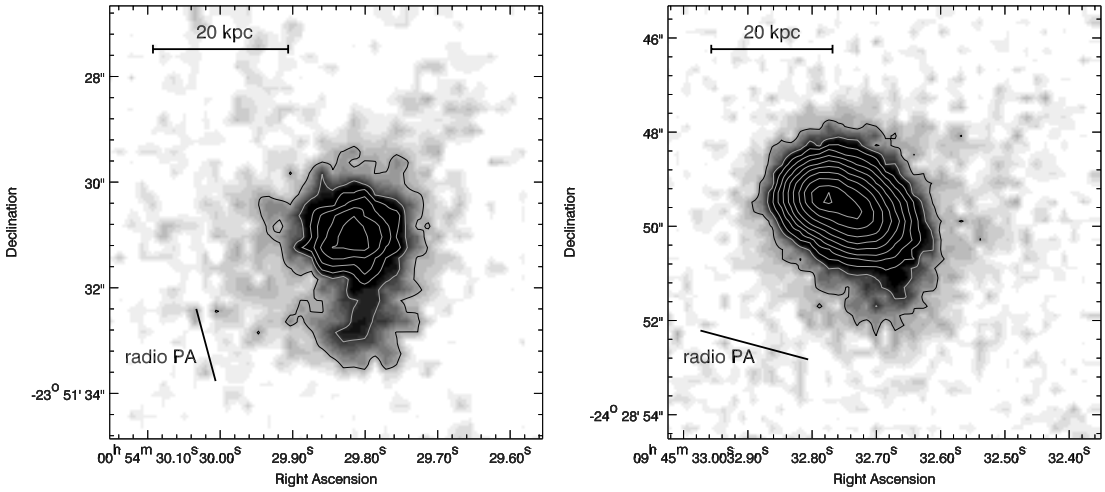

Fig. 15. Same as Fig. 14, but showing the halos of the radio galaxies MRC 0052–241 (*left*) and MRC 0943–242 (*right*).

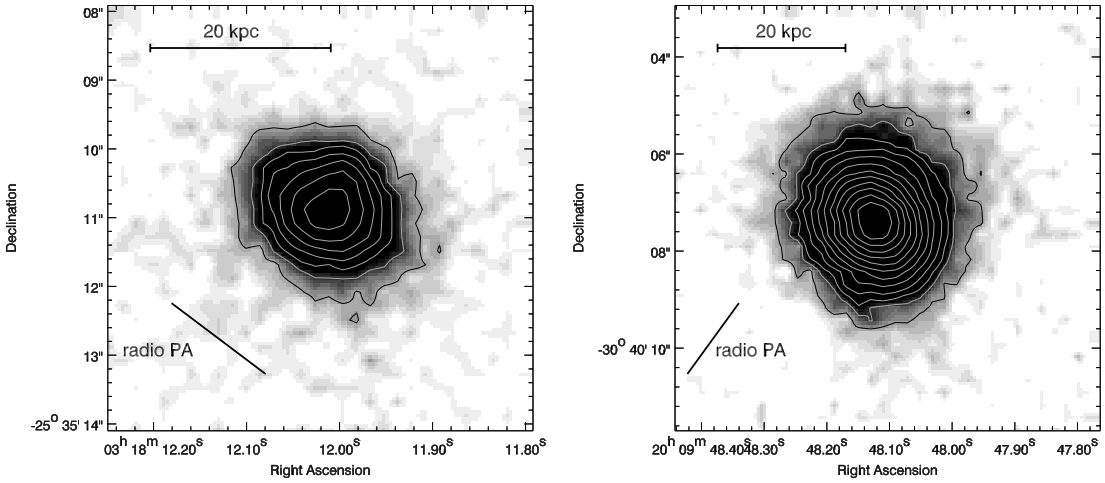

Fig. 16. Same as Fig. 14, but showing the halos of the radio galaxies MRC 0316–257 (*left*) and TN J2009–3040 (*right*).

luminosities ranging between 10^{43} and a few times 10^{45} erg s^{-1}. The continuum subtracted Lyα images of the radio galaxies observed in our VLT program are shown in Figs. 14−17. The region from which the Lyα emission originates is spatially resolved and the emission line halos can be seen over 150 kpc in some cases. In Table 5, we summarize the luminosity, size and position angles of the halos.

The position angles of the emission line halos and the radio emission are aligned, with the difference in the angle generally less than ∼20° (see Table 5). This alignment between

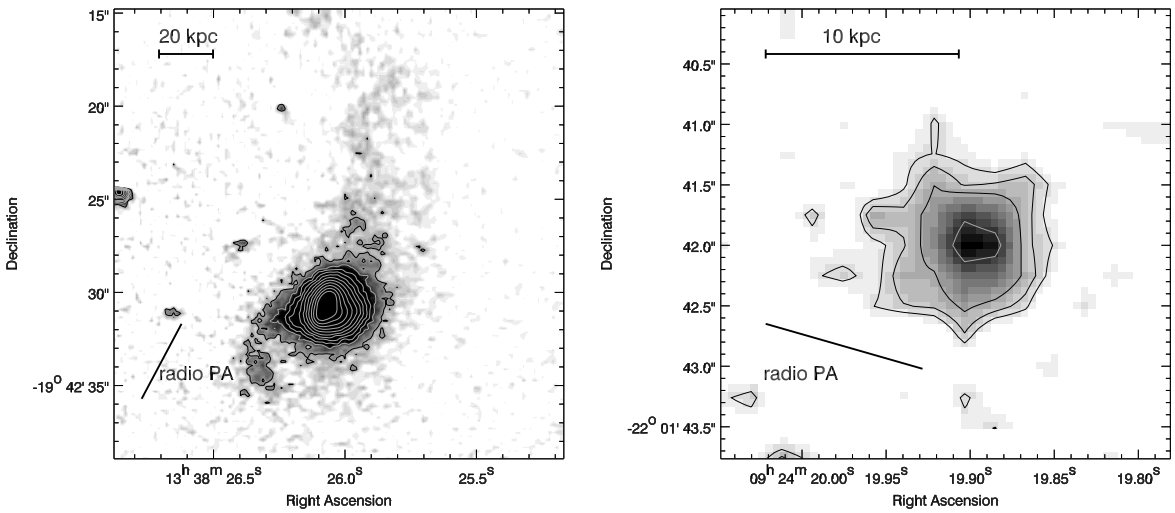

Fig. 17. Same as Fig. 14, but showing the halos of the radio galaxies TN J1338–1942 (*left*) and TN J0924–2201 (*right*).

Table 5. Luminosity, size and position angle (PA) of the Lyα halos surrounding the radio galaxies observed in our VLT program. The position angles of the halos are measured from the Lyα images (Figs. 14–17) and are accurate to ∼10 degrees.

Name	$L_{\mathrm{Ly}\alpha}$ erg s^{-1}	Size kpc×kpc	PA halo deg[a]	PA radio deg[a]
BRL 1602–174	7.5×10^{44}	90×55	60	56[b]
MRC 2048–272	6.5×10^{43}	70×40	25	42[b]
MRC 1138–262	2.5×10^{45}	250×125	74	98[b]
MRC 0052–241	7.5×10^{43}	35×30	5	15[b]
MRC 0943–242	2.5×10^{44}	50×40	55	74[b]
MRC 0316–257	7.0×10^{43}	35×25	55	53[b]
TN J2009–3040	3.0×10^{44}	40×40	–[c]	144[b]
TN J1338–1942	4.5×10^{44}	130×45	170	152[b]
TN J0924–2201	1.5×10^{43}	10×10	90	74[b]

[a] Position Angle in degrees, measured east of north.
[b] References for the radio position angles: Best et al. (1999) (1602), Pentericci et al. (2000b) (2048), Pentericci et al. (1997) (1138), Kapahi et al. (1998) (0052), Pentericci et al. (1999) (0943), Carilli et al. (1997) (0316), De Breuck et al. (2000) (2009, 1338 and 0924).
[c] The halo of TN J2009–3040 is circular.

the emission line halo and the radio jet is a common feature in radio galaxies (e.g. McCarthy 1993; van Ojik et al. 1996; Pentericci et al. 1997; Reuland et al. 2003), and suggests that a least part of the Lyα emission is caused by the interaction of the gas with the radio jet or by ionisation by the photon beam that is aligned with the radio jet. See for a detailed analysis of the halos of the radio galaxies 1138 and 1338 the papers of Pentericci et al. (1997) and Zirm et al. (2005) respectively. Because an extensive study of the gas halos surrounding the other radio galaxies is beyond the scope of this article, we will present those results in a separate paper (Humphrey et al. in prep).

It is interesting to mention that we do not find (angular) clustering of Lyα emitters along the axes of the radio sources. This so-called "companion alignment" has been predicted by models (e.g. West 1994) and statistical detections of this effect using number counts have been reported by various authors (e.g. Röttgering et al. 1996; Bornancini et al. 2006). In contrast, the spatial distribution of the Lyα emitters near the radio galaxies studied in our program is rather homogeneous throughout the field (e.g. Figs. 4, 7, and Fig. 19 in V05). Recently, Croft et al. (2005) reported that near 1138 at least three spectroscopically confirmed, X-ray selected AGN are, together with the radio galaxy, members of a filamentary structure of at least a few (proper) Mpc, in alignment with the radio jet axis. The Lyα emitters in this protocluster do not show such a clear alignment (Kurk et al. 2004b). It is therefore possible that only certain types of galaxies, e.g. the more massive galaxies, are preferentially aligned with the radio galaxy axes, while the young and presumably less massive Lyα emitters (V05) do not show this angular clustering. Future observations, aimed detecting the different galaxy populations in the protoclusters, could test this picture.

4. The environment of high redshift radio galaxies

Besides the target of our pilot project, MRC 1138−262 at $z = 2.16$, we imaged areas surrounding eight radio galaxies with $2.0 < z < 5.2$. A total of 300 candidate Lyα emitters was selected fulfilling the selection criteria $EW_0 > 15$ Å and $\Sigma \equiv EW_0/\Delta EW_0 > 3$ (Tables 3 and 6). One field (BRL 1602−174 at $z = 2.04$) suffered from high galactic extinction and a low response of the CCD. We will discard this field in the following discussion. In the remaining seven radio galaxy fields spectra were taken of 152 candidates. These observations confirmed 139 Lyα emitters. The success rate of our selection procedure is ∼91%. Only nine candidates could not be confirmed spectroscopically. These candidates had a faint predicted line flux ($F_{\mathrm{Ly}\alpha} < 10^{-17}$ erg s^{-1} cm^{-2}) and the non-detections are most likely caused by a lack of signal-to-noise. An overview of the number of candidates, spectroscopically observed and confirmed Lyα emitters per field is given in Table 6.

Four candidate emitters were identified with low redshift objects. We estimate that the contamination of our (candidate) sample is roughly 3%, although this percentage varies strongly from field to field and with redshift. For example, the fraction of contaminants in the field surrounding TN J0924−2201 at $z = 5.2$ is 25% (Venemans et al. 2004), while in four fields near $z \sim 3$, the contamination fraction is ∼2% (see Table 6).

Fourteen objects that fell outside our selection criteria were also confirmed to be Lyα emitters, increasing the number of confirmed Lyα emitters to 153. Adding the 15 confirmed emitters in the 1138 field (Pentericci et al. 2000a), a total of 168 Lyα emitters are confirmed near eight high redshift radio galaxies.

Table 6. Summary of the results of the imaging and spectroscopic observations of the radio galaxy targets. For completeness, the target of the pilot project, MRC 1138–262 is included.

Field	z	$N^a_{\rm img}$	$N^b_{\rm spec}$	$N^c_{\rm conf}$	$N^d_{\rm none}$	$N^e_{{\rm low}\,z}$	$N^f_{\rm extra}$	$N^g_{\rm tot}$	$n_{\rm rg}/n^h_{\rm field}$	σ^i_v km s^{-1}	$M^j_{\rm pcl}$ $10^{14}\,M_\odot$
1602	2.04	2	–	–	–	–	–	–	–	–	–
2048	2.06	10	3	2	1	0	1	3	$1.2^{+0.8}_{-0.7}$	–	–
1138	2.16	37	11	11	0	0	4	15	4 ± 2	900 ± 240	3–4
0052	2.86	57	36	35	1	0	2	37	$3.0^{+0.5}_{-0.4}$	980 ± 120	3–4
0943	2.92	65	30	25	4	1	3	28	$3.2^{+0.9}_{-0.7}$	715 ± 105	4–5
0316	3.13	77	30	28	1	1	3	31	$3.3^{+0.5}_{-0.4}$	640 ± 195	3–5
2009	3.16	21	9	9	0	0	2	11	$1.7^{+0.8}_{-0.6}$	515 ± 90	–
1338	4.11	54	36	34	2	0	3	37	$4.8^{+1.1}_{-0.8}$	265 ± 65	6–9
0924	5.20	14	8	6	0	2	0	6	$2.5^{+1.6}_{-1.0}$	305 ± 110	4–9

[a] Number of candidate Lyα emitters with $EW_0 > 15$ Å and $EW_0/\Delta EW_0 > 3$. [b] Number of spectroscopically observed candidates. [c] Number of spectroscopically confirmed Lyα emitters. [d] Number of candidates not detected spectroscopically. [e] Number of low redshift emission line galaxies among the observed candidates. [f] Number of confirmed Lyα emitters not satisfying the imaging selection criteria. [g] Total number of confirmed Lyα emitters near the radio galaxy. [h] Density of the emitters as compared to the field density on the basis of the imaging candidates. Note that the redshift range of the confirmed emitters is generally smaller than the width of the filter (see Sects. 3 and 5.2). [i] Velocity dispersion of the confirmed emitters. [j] Estimated mass of the protocluster (Sect. 5.2).

Based on the (volume) overdensity and the clustering of emitters in redshift space, we argue that at least five of the radio galaxies (MRC 1138–262, MRC 0052–241, MRC 0943–242, MRC 0316–257 and TN J1338–1942) are associated with a forming cluster of galaxies (protocluster). We are not able to make a definite statement about the environment of TN J0924–2201 at $z = 5.2$, due to the small number of confirmed galaxies (Venemans et al. 2004). Recent multi-color observations with the *HST* indicate that this field is overdense (at the 99.6% level) in V-band dropouts (Overzier et al. 2006b), and these dropouts could represent an additional galaxy population in the protocluster. Although follow-up spectroscopy is needed to confirm that the dropouts are at $z = 5.2$, the richness of Lyman break galaxies in the field strengthens our hypothesis that a large structure is present at $z = 5.2$. The two remaining radio galaxy fields, the 2048 and 2009 fields, have Lyα volume densities consistent with the field density. In the 2009 field, clustering can be seen in the position of the emitters on the sky and in velocity space. More observations in this field are needed to confirm the clustering and to identify a possible structure of galaxies. Based on the results in the eight radio galaxy fields, 75% of luminous ($L_{2.7\,\rm GHz} > 10^{33}$ erg s^{-1} Hz^{-1} sr^{-1}) radio galaxies at $z > 2$ are associated with a forming cluster of galaxies.

In the next section, we will describe the properties of the radio galaxy protoclusters as a whole. The properties of the high redshift Lyα emitters are or will be discussed elsewhere (Kurk et al. 2004b; V05; Venemans et al. in prep.).

5. Properties of high redshift protoclusters

5.1. Structure size

As can be seen in Figs. 4, 7, 10 and 11, the sizes of the protoclusters are generally larger than the field of view of the FORS2 camera ($>3.2 \times 3.2$ Mpc^2). Only in the 1338 field a boundary can be seen to the north-west of the radio galaxy (but see below). Kurk et al. (2004b) found that the surface density of Lyα emitters decreased with increasing distance to the radio galaxy in their field. Within the limitations of the relatively small number of objects, we tested each of our fields to see whether there is a concentration of emitters near the radio galaxy. In two fields, the 0052 and 0316 fields, we found that density did not change with distance to the radio galaxy, and that the distribution of emitters was roughly homogeneous over the imaged area. Most likely, the extent of the protocluster in these fields is larger than the area covered by our imaging. In the 0943 field at $z = 2.9$, the surface density of Lyα emitters declines further away from the radio galaxy, as is shown in Fig. 18. At a proper distance of ~1.75 Mpc from the radio galaxy, the surface density of Lyα emitters is consistent with the field density. We regard this radius as the size of the protocluster. A similar distribution was found in the 1338 field, but only if the average position of the emitters was taken as centre (see Fig. 19). As mentioned in Sect. 3.8, the radio galaxy is located at a distance of 1.3 Mpc from the centre of the emitters. We estimate that the size of this protocluster is 2.0 Mpc (Fig. 19).

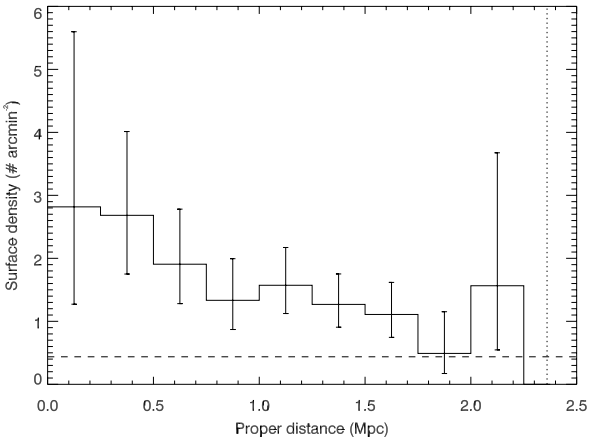

Fig. 18. Surface density of emitters as a function of proper distance from the radio galaxy MRC 0943–242. The error bars represent Poissonian errors. The horizontal dashed line is the surface density of Lyα emitters in blank fields. The vertical dotted line represents the maximum distance measurable in the image.

However, these size estimates of the protoclusters are based only on the position of Lyα emitters. It is possible that other galaxy populations in the protoclusters are distributed differently. As already mentioned in Sect. 3.8, an overdensity of mm galaxies is located to the north of the radio galaxy TN J1338−1942 (De Breuck et al. 2004), whereas the highest concentrations of Lyα emitters in this field lies south of

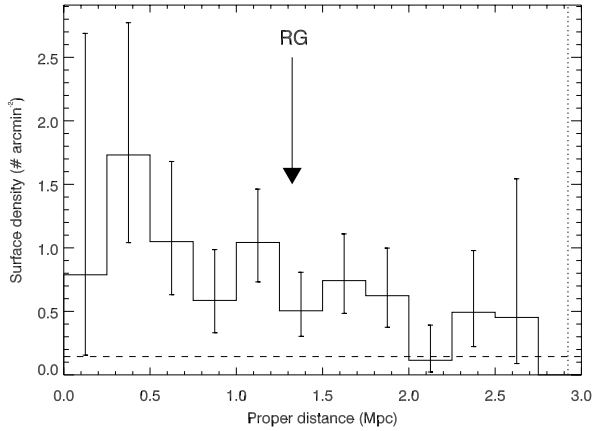

Fig. 19. Surface density of emitters as a function of proper distance from the average position of the emitters in the field near TN J1338–1942 at $z = 4.1$. The position of the radio galaxy is indicated by the arrow. The error bars represent Poissonian errors. The dashed line is the surface density of field Lyα emitters (Dawson et al. 2004; Shimasaku et al. 2004, see Sect. 3.8). The dotted line is the maximum distance measurable in our imaging.

the radio source. Also, Kurk et al. (2004b) found that in the 1138 protocluster at $z = 2.16$ the population of Hα emitters and EROs are more concentrated towards the radio galaxy than the Lyα emitters. Despite this caveat, our size (radius) estimates of >1.75−2.0 Mpc are consistent with the determination by other groups. For example, Keel et al. (1999) estimate that the large structure around the radio galaxy 53W002 at $z = 2.4$ has a diameter of ∼3.3 Mpc. Hayashino et al. (2004) imaged a protocluster at $z \sim 3.1$, that was serendipitously discovered by Steidel et al. (1998). They found that the region that is overdense in Lyα emitters has a size of approximately 5×5 Mpc^2. At a higher redshift, an overdensity of Lyα emitters at $z = 4.9$ was discovered by Shimasaku et al. (2003) in the SDF. This overdensity has a roughly circular shape with a radius of ∼2.0 Mpc (Shimasaku et al. 2003), which is very similar to the size of the 1338 protocluster.

To summarize, we find that the sizes of the protoclusters, as inferred by the distribution of Lyα emitters at $z = 2.9$ and $z = 4.1$, are roughly ∼2.0 Mpc. The other protoclusters do not show a boundary and could be larger. Wide field imaging is needed for these protoclusters to see a boundary of the galaxy distribution.

5.2. Mass

The age of the Universe at $z = 3$ is only ∼15% of its current age, which corresponds to ∼2 Gyr in our adopted cosmology. A protocluster galaxy with a relative velocity of 500 km s^{-1} would take at least 4 Gyr to cross a structure with a size of 2 Mpc. Therefore, the protoclusters are most likely still in the process of formation. They are still far from virialization and we cannot use the virial theorem to calculate the mass of the galaxy structures.

An alternative approach to calculate the mass of the structures is to assume that the mass that is located within the volume that is occupied by the protocluster galaxies will collapse into a single structure (see e.g., Steidel et al. 1998). To use this method we need to know the mass overdensity δ_m within the volume. The mass overdensity is related to the galaxy overdensity $\delta_{\rm gal}$ by the bias parameter $b \equiv \delta_{\rm gal}/\delta_m$.

To compute the volume of the protocluster, we estimate the redshift range of the confirmed Lyα emitters after removing outliers (galaxies more than ∼1500 km s^{-1} away from the median redshift). Because redshift space distortions modify the occupied volume, we corrected for peculiar velocities by assuming the structure is just breaking away from the Hubble flow (see Steidel et al. 1998; V05 for more details). If outliers are included, the volume occupied by the protoclusters increases and the estimated masses are higher.

Using this method, V05 estimate that the mass of the 0316 protocluster is $\sim5 \times 10^{14}$ $M_\odot$. Below we will estimate the mass of the protoclusters in the 1138, 0052, 0943, 1338 and 0924 fields. A bias parameter of $b = 3-6$ will be assumed, as suggested by e.g. Steidel et al. (1998) and Shimasaku et al. (2003).

• *1138:* near the radio galaxy MRC 1138−262, the overdensity of emitters in a comoving volume of 4490 Mpc^3 is $\delta_{\rm gal} > 3.4$ (Pentericci et al. 2000a; Kurk et al. 2004b). The computed mass in this volume is at least $3-4 \times 10^{14}$ $M_\odot$.

Interestingly, the redshift distribution of the Lyα emitters in this field appears to be bimodal (Pentericci et al. 2000a). The emitters are located in two subgroups with velocity dispersions 520 and 280 km s^{-1} (Pentericci et al. 2000a). Calculating the mass of the individual groups gives $\sim2\times10^{14}$ and $1-2\times10^{14}$ $M_\odot$. If the galaxies in these two groups are close to virialization, we can apply the virial theorem. Kurk et al. (2004b) estimated that the virial radii of the two groups is ∼1 Mpc. Using the velocity dispersions as given by Pentericci et al. (2000a), the virial masses of the groups are 4.0×10^{14} and 1.0×10^{14} $M_\odot$, comparable to the other estimates.

• *0052:* to estimate the volume that most likely will collapse into a single structure, we removed the three lowest and the two highest redshift galaxies. These galaxies are on the edges of the redshift distribution (Fig. 4), and we regard them as outliers. The remaining 32 emitters have redshifts in the range $2.8437 \leq z \leq 2.8673$. The range of $\Delta z = 0.0236$ is a factor 2.3 smaller than the redshift range probed by the narrow-band filter ($\Delta z = 0.0541$). The volume occupied by the emitters is 3510 comoving Mpc^3 (uncorrected for peculiar velocities). The overdensity within the volume is $0.0541/0.0236 \times 32/37 \times 3.0 = 5.95$. Using these values, the estimated mass is $3-4 \times 10^{14}$ $M_\odot$. Because the field of view of our imaging is not large enough to show a boundary of the structure (Fig. 4), this mass is a lower limit.

As in the 1138 field, the emitters are concentrated in two velocity groups (see Fig. 4). The groups consist of 12 and 19 members and have velocity dispersions of 185 and 230 km s^{-1} respectively. Assuming that the virial theorem can be applied for the two groups, this gives masses of 1.1×10^{14} and 7×10^{13} $M_\odot$ for the groups. Most likely, the mass of the protocluster lies in the range $2-4 \times 10^{14}$ $M_\odot$.

• *0943:* the redshift range of the confirmed emitters is 0.034, and, as described in Sect. 5.1, the size of the structure is roughly 1.75 Mpc in radius. This gives a comoving volume of 4570 Mpc^3. Within this volume 61 of the 65 emitters (94%) are located. The overdensity of emitters in this volume is 5.5, giving a protocluster mass of $4-5 \times 10^{14}$ $M_\odot$. Because the protocluster might extend towards lower redshifts (see Fig. 7), this mass must be regarded as a lower limit.

• *1338:* the $z = 4.1$ protocluster has a size of 2 Mpc in radius (Sect. 5.1), giving an area that is 78% of the total area observed (Fig. 11). The fraction of (candidate) emitters in this area is 91%. The volume occupied by these emitters is 5815 Mpc^3. The overdensity of emitters in this volume is ∼8.5, resulting in a mass of $6-9 \times 10^{14}$ $M_\odot$.

• *0924:* the redshifts of the confirmed emitters near TN J0924–2201 only span a relatively narrow redshift range

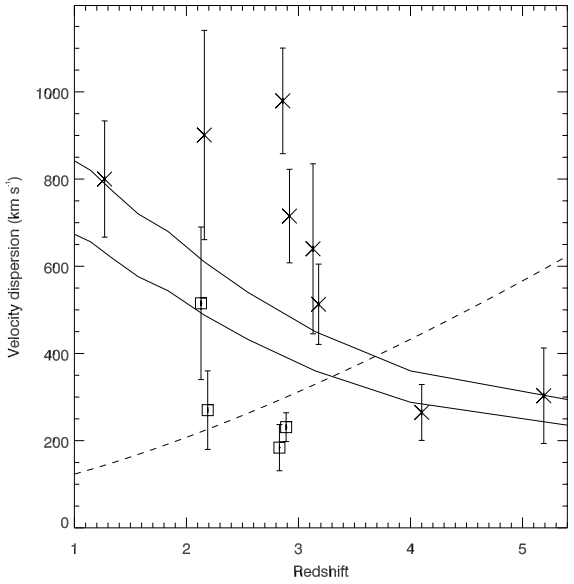

Fig. 20. Velocity dispersion of Lyα emitters in our radio galaxy fields (*crosses*) as a function of redshift. The squares represent the velocity dispersions of the subgroups in the 1138 and 0052 fields (see Sect. 5.2). The data point near $z = 1$ represents the velocity dispersion in the X-ray cluster RDCS 1252.9-2927 at $z = 1.24$ (Rosati et al. 2004). The dashed line is the Hubble flow $H(z)$ over 1 Mpc. The solid lines show the evolution of the dark matter velocity dispersions $\sigma_{\rm dm}$ of simulated massive clusters (Eke et al. 1998). The top line is scaled to 1000 km s^{-1} at $z = 0$, the bottom line to 800 km s^{-1} at $z = 0$.

of $\Delta z = 0.0151$ (Venemans et al. 2004). The corresponding volume is 1870 Mpc^3 and the density of emitters as compared to the field density in this volume is 20.3. The structure mass is estimated to be $4{-}6 \times 10^{14}$ $M_\odot$, although the small number of confirmed emitters makes this mass quite uncertain.

The mass estimates of the protoclusters are in the range $2{-}9 \times 10^{14}$ $M_\odot$. Locally, such masses correspond to clusters with Abell richness class 0 and higher (e.g., Bahcall & Cen 1993). This indicates that the protoclusters are the progenitors of present-day massive clusters.

5.3. Velocity dispersions

In Fig. 20, the velocity dispersion of the Lyα emitters in the radio galaxy fields are plotted as a function of redshift. Despite the small number of data points, the dispersion appears to increase with decreasing redshift. While at $z > 4$ the velocity dispersion is $\sim$300 km s^{-1}, the dispersion increases to 500$-$700 km s^{-1} at $z \sim 3$. In our two lowest redshift fields ($z = 2.86$ and $z = 2.16$), the velocity dispersion of the emitters is 1000 km s^{-1}. However, it should be noted that the velocity distribution of emitters at $z = 2.86$ and $z = 2.16$ is bimodal (Sect. 5.2), and the velocity dispersion of the individual subgroups is much lower (200$-$500 km s^{-1}). Numerical simulations of the evolution of massive clusters predict that the velocity dispersion of the dark matter increases with cosmic time (e.g., Eke et al. 1998). Although based on only one population of galaxies in the protoclusters, our observations are consistent with these predictions. Our data approximately follow the evolution of a massive cluster of galaxies, with a velocity dispersion of 1000 km s^{-1} at $z = 0$ (Fig. 20). Additional observations of high redshift protoclusters are needed to confirm this.

6. Discussion

A question is whether the radio galaxy selected protoclusters presented in this paper are biased. To answer this question, we have to assess the number density of powerful radio galaxies at $z > 2$.

The radio galaxies in our program have luminosities $L_{2.7\,\rm GHz} > 10^{33}$ erg s^{-1} Hz^{-1} sr^{-1} (Table 1). The number density of radio sources with this luminosity limit in the redshift range $2 < z < 5$ is 4×10^{-8} Mpc^{-3} (Dunlop & Peacock 1990). Using the more recent radio luminosity function at 151 MHz as derived by Willott et al. (2001) and assuming a spectral slope of $\alpha \simeq -1.0$ gives a number density that is similar within a factor of 2. It should be noted that the number density depends strongly on the lower luminosity limit that is assumed, since the density varies approximately with $n \propto L^{-2}$ (Dunlop & Peacock 1990).

The association of 75% of $z > 2$ radio galaxies with a protocluster (Sect. 4) implies that there are roughly 3×10^{-8} forming clusters at $2.0 < z < 5.2$ per comoving Mpc^3 with an active radio source. However, it is likely that there will be many more forming clusters in this redshift range without an active radio source. Blundell & Rawlings (1999) argue that high redshift radio galaxies are visible only when they are younger than 10^7 yr. Between $z = 5.2$ and $z = 2$, the age of the Universe increases with roughly 2 Gyr. This means that between $z = 5.2$ and $z = 2$, there must be a factor $\sim 2 \times 10^2$ more forming clusters *without* a bright radio source. Therefore, most high redshift protoclusters will not have a powerful radio galaxy.

Based on these calculations, we estimate that the number density of protoclusters such as the ones presented in this paper is $\sim 6 \times 10^{-6}$ Mpc^{-3}. It is instructive to compare this number with the density of protoclusters as derived by other groups. Steidel et al. (1998) estimate that they find one galaxy overdensity in a $9' \times 18'$ field in a redshift range $2.7 < z < 3.4$ in their Lyman break galaxy survey. In our cosmology, this translates to a number density of protoclusters of 3×10^{-6} Mpc^{-3}. High redshift blank field Lyα searches also found several galaxy overdensities. Shimasaku et al. (2003) reports the discovery of a structure of Lyα emitters at $z = 4.9$ in the Subaru Deep Field with an estimated mass of 3×10^{14} $M_\odot$. The implied volume density of such structures is 7×10^{-6} Mpc^{-3}. At even higher redshifts, Ouchi et al. (2005) find two overdensities of Lyα emitters at $z = 5.7$ in a 1.0 deg^2 region of the sky. They estimate a density of $> 2 \times 10^{-6}$ Mpc^{-3} for such structures. These blank field density estimates are very similar to our calculated density of $\sim 6 \times 10^{-6}$ Mpc^{-3}. This indicates that the overdensities discovered in blank field surveys and our protoclusters near radio galaxies could very well be the same type of object. It is likely that we see the protocluster at the time that the brightest cluster galaxy undergoes a burst of nuclear activity.

Interestingly, in the local Universe objects with a similar volume density as the protoclusters are clusters with masses $\gtrsim 2 \times 10^{14}$ $M_\odot$ (Girardi et al. 1998; Reiprich & Böhringer 2002), which compares favourably with the mass estimates presented in Sect. 5.2. This further supports the idea that the protoclusters are the progenitors of (rich) clusters of galaxies.

7. Summary

In this paper we have presented the results of a large observational program to search for galaxy overdensities near luminous radio galaxies at $2 < z < 5.2$. The targets for our project were selected from a list of roughly 150 $z > 2$ radio sources, and were required to be luminous in the radio

with $L_{2.7\,\mathrm{GHz}} > 10^{33}$ erg s^{-1} Hz^{-1} sr^{-1} and to have redshifts and positions optimum for deep narrow-band Lyα imaging with the FORS2 camera on the VLT. We selected three radio galaxies at $z \simeq 2.1$ (including the target of our pilot project MRC 1138−262), two at $z \simeq 2.9$, two at $z \simeq 3.1$, one at $z = 4.1$ and one at $z = 5.2$.

To search for Lyα emitting galaxies at the redshift of the radio galaxies, we obtained deep narrow-band Lyα and broad-band images with the VLT and the Keck telescope of the fields surrounding the radio galaxies. The size of the images was roughly $6\farcm8 \times 6\farcm8$, which corresponds at a redshift of 3 to a proper size of 3.1×3.1 Mpc^2. The (typical) sensitivity reached in the imaging is a Lyα luminosity of $L_{\mathrm{Ly}\alpha} \sim 10^{42}$ erg s^{-1} for an emitter with no continuum detected at the 5σ level in the narrow-band image. An exception is the field of BRL 1602−174 at $z = 2.04$, the lowest redshift radio galaxy in our program. Due to the high galactic extinction towards this radio source and the low quantum efficiency of the FORS2 detector at the wavelengths below 4000 Å, the imaging of this field was significant shallower than of the other fields and therefore only two candidate emitters were detected. No follow-up spectroscopy was conducted in this field. Using the narrow-band and broad-band images we found 300 candidate Lyα emitters with a rest-frame equivalent width of $EW_0 > 15$ Å and a significance $\Sigma \equiv EW_0/\Delta EW_0 > 3$.

To confirm whether these candidate emitters have redshifts similar to that of the radio galaxies, we conducted follow-up spectroscopy with the VLT and Keck. Candidate emitters were confirmed to be Lyα emitters based on an observed (asymmetric) line profile, emission line ratios and/or continuum break. Of the 152 candidate Lyα emitters observed spectroscopically, 139 (91%) were confirmed to be Lyα emitters, four (3%) were low redshift interlopers and nine (6%) did not show a line (or continuum) in their spectra, which is most likely due to a lack of signal-to-noise. Furthermore, 14 sources that were not selected as emitters were also confirmed to be high redshift Lyα emitters. Combined with the 15 emitters found near MRC 1138–262, the total number of confirmed Lyα emitters is 168 in eight radio galaxies fields. We will describe the properties of these Lyα emitters in a forthcoming paper (Venemans et al. in prep).

Six of the fields are overdense in Lyα emitters by a factor of 3−5 as compared to the volume density of (field) Lyα emitters at similar redshifts. The remaining two radio galaxy fields have volume densities that are within the errors consistent with the field density. The significance of the volume overdensity near our highest redshift radio galaxy, at $z = 5.2$, is only marginal due to the low number (six) of confirmed emitters. Recently, an overdensity of LBGs was found in this field using multi-color *HST* observations. This strengthens our hypothesis that the radio galaxy is located in an overdense region.

The confirmed emitters show clustering in redshift space, and the width of the redshift distribution of the confirmed emitters is a factor 2−5 smaller than the width of the narrow-band filters. Taken together with the volume overdensity of Lyα emitters, we argue that six of the radio galaxies reside in a forming cluster of galaxies or protocluster. We estimate that of all powerful high redshift radio galaxies at least $6/8 = 75\%$ are located in a protocluster, making our program very efficient in finding high redshift forming clusters.

The size of the protoclusters is, based on the distribution of Lyα emitters, at least 1.75 Mpc. This is consistent with the size measurements by other groups. The mass of the protoclusters can be calculated assuming the galaxies in the protoclusters are just breaking away from the Hubble flow and that the mass inside the volume occupied by the protocluster galaxies will collapse into a single structure. This method yields masses in the range $2-9 \times 10^{14}$ $M_\odot$, suggesting that the protoclusters are the progenitors of clusters with Abell richness class 0 or higher. The results of our program allows us to follow the evolution of the velocity dispersion of the Lyα emitters in the overdense regions as a function of redshift. Although based on only a small number of data points, we find that the velocity dispersion increases with decreasing redshift, in agreement with the predictions of numerical simulations of forming clusters. In a future paper, we will present a more detailed comparison of our observations with numerical simulations of forming massive clusters (Venemans et al. in prep).

Based on the results of our program and the density of luminous radio sources at $z > 2$ and assuming that radio galaxies at high redshift are visible only for 10^7 yr, we estimate that the number density of protoclusters at $2 < z < 5.2$ is 6×10^{-6} Mpc^{-3}. Locally, objects that have such number densities are clusters of galaxies with masses in excess of 2×10^{14} $M_\odot$. This further supports the idea that the protoclusters are the progenitors of (rich) clusters of galaxies. Using the protoclusters presented in this paper, we are now able to systematically study the evolution of clusters and their galaxies out to redshifts $z > 5$.

Acknowledgements. We are grateful to the staff of Paranal, Chile, for their excellent support. We thank Gero Rupprecht at ESO and William Grenier of Andover Corporation for their help in our purchase of the custom narrow-band filters. BPV thanks Michiel Reuland, Hyron Spinrad, Steve Dawson and Curtis Manning for useful discussions, and Philip Best for carefully reading an early draft of this manuscript. GKM acknowledges funding by an Academy Professorship of the Royal Netherlands Academy of Arts and Sciences (KNAW). The work by WvB, SC and SAS at LLNL was performed under the auspices of the US Department of Energy, National Nuclear Security Administration, by the University of California, Lawrence Livermore National Laboratory under contract No. W-7405-Eng-48. The authors wish to recognize and acknowledge the very significant cultural role and reverence that the summit of Mauna Kea has always had within the indigenous Hawaiian community. We are most fortunate to have the opportunity to conduct observations from this mountain. This research has made use of the NASA/IPAC Extragalactic Database (NED) which is operated by the Jet Propulsion Laboratory, California Institute of Technology, under contract with the National Aeronautics and Space Administration. This work was supported by the European Community Research and Training Network "The physics of the Intergalactic Medium". SC and WvB acknowledge support for radio galaxy studies at UC Merced, including the work reported here, with the Hubble, Spitzer and Chandra space telescopes via NASA grants HST 10127, SST 3482, SST 3329 and CXO 06701011.

References

Appenzeller, I., & Rupprecht, G. 1992, The Messenger, 67, 18
Archibald, E. N., Dunlop, J. S., Hughes, D. H., et al. 2001, MNRAS, 323, 417
Athreya, R. M., Kapahi, V. K., McCarthy, P. J., & van Breugel, W. J. M. 1998, A&A, 329, 809
Bahcall, N. A., & Cen, R. 1993, ApJ, 407, L49
Bahcall, N. A. & Fan, X. 1998, ApJ, 504, 1
Bahcall, N. A., Fan, X., & Cen, R. 1997, ApJ, 485, L53
Baldwin, J. A., & Stone, R. P. S. 1984, MNRAS, 206, 241
Barr, J. M., Baker, J. C., Bremer, M. N., Hunstead, R. W., & Bland-Hawthorn, J. 2004, AJ, 128, 2660
Beers, T. C., Flynn, K., & Gebhardt, K. 1990, AJ, 100, 32
Bertin, E., & Arnouts, S. 1996, A&AS, 117, 393
Bessell, M. S. 1979, PASP, 91, 589
Best, P. N. 2000, MNRAS, 317, 720
Best, P. N., Röttgering, H. J. A., & Lehnert, M. D. 1999, MNRAS, 310, 223
Best, P. N., Lehnert, M. D., Miley, G. K., & Röttgering, H. J. A. 2003, MNRAS, 343, 1
Blakeslee, J. P., Franx, M., Postman, M., et al. 2003, ApJ, 596, L143
Blundell, K. M., & Rawlings, S. 1999, Nature, 399, 330
Bornancini, C. G., Lambas, D. G., & De Breuck, C. 2006, MNRAS, 366, 1067
Carilli, C. L., Röttgering, H. J. A., van Ojik, R., Miley, G. K., & van Breugel, W. J. M. 1997, ApJS, 109, 1
Carilli, C. L., Miley, G., Röttgering, H. J. A., et al. 2001, in ASP Conf. Ser., 101

Carlstrom, J. E., Holder, G. P., & Reese, E. D. 2002, ARA&A, 40, 643
Ciardullo, R., Feldmeier, J. J., Krelove, K., Jacoby, G. H., & Gronwall, C. 2002, ApJ, 566, 784
Cooke, J., Wolfe, A. M., Prochaska, J. X., & Gawiser, E. 2005, ApJ, 621, 596
Croft, S., Kurk, J., van Breugel, W., et al. 2005, AJ, 130, 867
Dawson, S., Rhoads, J. E., Malhotra, S., et al. 2004, ApJ, 617, 707
De Breuck, C., van Breugel, W. J. M., Minniti, D., et al. 1999, A&A, 352, L51
De Breuck, C., van Breugel, W., Röttgering, H. J. A., & Miley, G. 2000, A&AS, 143, 303
De Breuck, C., van Breugel, W. J. M., Röttgering, H., et al. 2001, AJ, 121, 1241
De Breuck, C., van Breugel, W. J. M., Stanford, S. A., et al. 2002, AJ, 123, 637
De Breuck, C., Neri, R., Morganti, R., et al. 2003a, A&A, 401, 911
De Breuck, C., Neri, R., & Omont, A. 2003b, New Astron. Rev., 47, 285
De Breuck, C., Bertoldi, F., Carilli, C., et al. 2004, A&A, 424, 1
Deutsch, E. W. 1999, AJ, 118, 1882
Dey, A., van Breugel, W. J. M., Vacca, W. D., & Antonucci, R. 1997, ApJ, 490, 698
Dunlop, J. S., & Peacock, J. A. 1990, MNRAS, 247, 19
Eggen, O. J., Lynden-Bell, D., & Sandage, A. R. 1962, ApJ, 136, 748
Eke, V. R., Cole, S., & Frenk, C. S. 1996, MNRAS, 282, 263
Eke, V. R., Navarro, J. F., & Frenk, C. S. 1998, ApJ, 503, 569
Ellis, R. S., Smail, I., Dressler, A., et al. 1997, ApJ, 483, 582
Ettori, S., Tozzi, P., & Rosati, P. 2003, A&A, 398, 879
Fynbo, J. P. U., Møller, P., & Thomsen, B. 2001, A&A, 374, 443
Fynbo, J. P. U., Ledoux, C., Møller, P., Thomsen, B., & Burud, I. 2003, A&A, 407, 147
Gehrels, N. 1986, ApJ, 303, 336
Girardi, M., Borgani, S., Giuricin, G., Mardirossian, F., & Mezzetti, M. 1998, ApJ, 506, 45
Gladders, M. D. 2002, Ph.D. Thesis
Goto, T. 2005, MNRAS, 356, L6
Hall, P. B., Sawicki, M., Martini, P., et al. 2001, AJ, 121, 1840
Hammer, F., Flores, H., Lilly, S. J., et al. 1997, ApJ, 481, 49
Hashimoto, Y., Barcons, X., Böhringer, H., et al. 2004, A&A, 417, 819
Hayashino, T., Matsuda, Y., Tamura, H., et al. 2004, AJ, 128, 2073
Holden, B. P., van der Wel, A., Franx, M., et al. 2005, ApJ, 620, L83
Hu, E. M., Cowie, L. L., Capak, P., et al. 2004, AJ, 127, 563
Jarvis, M. J., Rawlings, S., Eales, S., et al. 2001, MNRAS, 326, 1585
Jarvis, M. J., Wilman, R. J., Röttgering, H. J. A., & Binette, L. 2003, MNRAS, 338, 263
Kapahi, V. K., Athreya, R. M., van Breugel, W., McCarthy, P. J., & Subrahmanya, C. R. 1998, ApJS, 118, 275
Keel, W. C., Cohen, S. H., Windhorst, R. A., & Waddington, I. 1999, AJ, 118, 2547
Kodaira, K., Taniguchi, Y., Kashikawa, N., et al. 2003, PASJ, 55, L17
Kurk, J. D., Röttgering, H. J. A., Pentericci, L., et al. 2000, A&A, 358, L1
Kurk, J. D., Pentericci, L., Overzier, R. A., Röttgering, H. J. A., & Miley, G. K. 2004a, A&A, 428, 817
Kurk, J. D., Pentericci, L., Röttgering, H. J. A., & Miley, G. K. 2004b, A&A, 428, 793
Landolt, A. U. 1992, AJ, 104, 340
Larson, R. B. 1974, MNRAS, 166, 585
Large, M. I., Mills, B. Y., Little, A. G., Crawford, D. F., & Sutton, J. M. 1981, MNRAS, 194, 693
Le Fèvre, O., Deltorn, J. M., Crampton, D., & Dickinson, M. 1996, ApJ, 471, L11
Ma, C., & Feissel, M. 1998, VizieR Online Data Catalog, 1251, 0
Madau, P. 1995, ApJ, 441, 18
Maughan, B. J., Jones, L. R., Ebeling, H., & Scharf, C. 2004, MNRAS, 351, 1193
McCarthy, P. J. 1993, ARA&A, 31, 639
McCarthy, P. J., Kapahi, V. K., van Breugel, W. J. M., & Subrahmanya, C. R. 1990, AJ, 100, 1014
McCarthy, P. J., Kapahi, V. K., van Breugel, W., et al. 1996, ApJS, 107, 19
McCarthy, J. K., Cohen, J. G., Butcher, B., et al. 1998, in Optical Astronomical Instrumentation, ed. S. D'Odorico, Proc. SPIE, 3355, 81
Miles, T. A., Raychaudhury, S., Forbes, D. A., et al. 2004, MNRAS, 355, 785
Miley, G. K., Overzier, R. A., Tsvetanov, Z. I., et al. 2004, Nature, 427, 47
Monaco, P., Moller, P., Fynbo, J., et al. 2005, A&A, 440, 799
Monet, D. G. 1998, BA&AS, 30, 1427
Monet, D. B. A., Canzian, B., Dahn, C., et al. 1998, VizieR Online Data Catalog, 1252, 0
Mullis, C. R., Rosati, P., Lamer, G., et al. 2005, ApJ, 623, L85
Nakata, F., Kajisawa, M., Yamada, T., et al. 2001, PASJ, 53, 1139
Nakata, F., Bower, R. G., Balogh, M. L., & Wilman, D. J. 2005, MNRAS, 357, 679
Norman, C., Hasinger, G., Giacconi, R., et al. 2002, ApJ, 571, 218
Oke, J. B. 1974, ApJS, 27, 21
Oke, J. B. 1990, AJ, 99, 1621
Oke, J. B., Cohen, J. G., Carr, M., et al. 1995, PASP, 107, 375
Ouchi, M., Shimasaku, K., Furusawa, H., et al. 2003, ApJ, 582, 60
Ouchi, M., Shimasaku, K., Akiyama, M., et al. 2005, ApJ, 620, L1
Overzier, R. A., Bouwens, R. J., Cross, N. J. G., et al. 2006a, ApJ, submitted [arXiv:astro-ph/0601223]
Overzier, R. A., Zirm, A. W., Miley, G. K., et al. 2006b, ApJ, 637, 58
Papadopoulos, P. P., Röttgering, H. J. A., van der Werf, P. P., et al. 2000, ApJ, 528, 626
Pascarelle, S. M., Windhorst, R. A., Driver, S. P., Ostrander, E. J., & Keel, W. C. 1996, ApJ, 456, L21
Pentericci, L., Röttgering, H. J. A., Miley, G. K., Carilli, C. L., & McCarthy, P. 1997, A&A, 326, 580
Pentericci, L., Röttgering, H. J. A., Miley, G. K., et al. 1998, ApJ, 504, 139
Pentericci, L., Röttgering, H. J. A., Miley, G. K., et al. 1999, A&A, 341, 329
Pentericci, L., Kurk, J. D., Röttgering, H. J. A., et al. 2000a, A&A, 361, L25
Pentericci, L., Van Reeven, W., Carilli, C. L., Röttgering, H. J. A., & Miley, G. K. 2000b, A&AS, 145, 121
Pentericci, L., McCarthy, P. J., Röttgering, H. J. A., et al. 2001, ApJS, 135, 63
Pentericci, L., Kurk, J. D., Carilli, C. L., et al. 2002, A&A, 396, 109
Reiprich, T. H., & Böhringer, H. 2002, ApJ, 567, 716
Reuland, M., van Breugel, W. J. M., Röttgering, H. J. A., et al. 2003, ApJ, 592, 755
Reuland, M., Röttgering, H., van Breugel, W., & De Breuck, C. 2004, MNRAS, 353, 377
Rhoads, J. E., Malhotra, S., Dey, A., et al. 2000, ApJ, 545, L85
Rhoads, J. E., Dey, A., Malhotra, S., et al. 2003, AJ, 125, 1006
Rhoads, J. E., Xu, C., Dawson, S., et al. 2004, ApJ, 611, 59
Rosati, P., Tozzi, P., Ettori, S., et al. 2004, AJ, 127, 230
Röttgering, H. J. A., Hunstead, R. W., Miley, G. K., van Ojik, R., & Wieringa, M. H. 1995, MNRAS, 277, 389
Röttgering, H. J. A., West, M. J., Miley, G. K., & Chambers, K. C. 1996, A&A, 307, 376
Röttgering, H. J. A., van Ojik, R., Miley, G. K., et al. 1997, A&A, 326, 505
Sánchez, S. F., & González-Serrano, J. I. 1999, A&A, 352, 383
Sánchez, S. F., & González-Serrano, J. I. 2002, A&A, 396, 773
Schlegel, D. J., Finkbeiner, D. P., & Davis, M. 1998, ApJ, 500, 525
Shimasaku, K., Ouchi, M., Okamura, S., et al. 2003, ApJ, 586, L111
Shimasaku, K., Hayashino, T., Matsuda, Y., et al. 2004, ApJ, 605, L93
Smith, J. A., Tucker, D. L., Kent, S., et al. 2002, AJ, 123, 2121
Somerville, R. S., Lee, K., Ferguson, H. C., et al. 2004, ApJ, 600, L171
Stanford, S. A., Eisenhardt, P. R., & Dickinson, M. 1998, ApJ, 492, 461
Steidel, C. C., Adelberger, K. L., Dickinson, M., et al. 1998, ApJ, 492, 428
Steidel, C. C., Shapley, A. E., Pettini, M., et al. 2004, ApJ, 604, 534
Steidel, C. C., Adelberger, K. L., Shapley, A. E., et al. 2005, ApJ, 626, 44
Stern, D., Bunker, A., Spinrad, H., & Dey, A. 2000, ApJ, 537, 73
Stevens, J. A., Ivison, R. J., Dunlop, J. S., et al. 2003, Nature, 425, 264
Stiavelli, M., Scarlata, C., Panagia, N., et al. 2001, ApJ, 561, L37
Stone, R. P. S., & Baldwin, J. A. 1983, MNRAS, 204, 347
Tanaka, M., Goto, T., Okamura, S., Shimasaku, K., & Brinkmann, J. 2004, AJ, 128, 2677
Tapken, C., Appenzeller, I., Mehlert, D., Noll, S., & Richling, S. 2004, A&A, 416, L1
Terlevich, R., Melnick, J., Masegosa, J., Moles, M., & Copetti, M. V. F. 1991, A&AS, 91, 285
Tozzi, P., Rosati, P., Ettori, S., et al. 2003, ApJ, 593, 705
Tran, K. H., van Dokkum, P., Illingworth, G. D., et al. 2005, ApJ, 619, 134
van Breugel, W., De Breuck, C., Stanford, S. A., et al. 1999, ApJ, 518, L61
van Dokkum, P. G., & Stanford, S. A. 2003, ApJ, 585, 78
van Ojik, R., Röttgering, H. J. A., Carilli, C. L., et al. 1996, A&A, 313, 25
van Zee, L., Barton, E. J., & Skillman, E. D. 2004, AJ, 128, 2797
Venemans, B. P., Kurk, J. D., Miley, G. K., et al. 2002, ApJ, 569, L11
Venemans, B. P., Röttgering, H. J. A., Overzier, R. A., et al. 2004, A&A, 424, L17
Venemans, B. P., Röttgering, H. J. A., Miley, G. K., et al. 2005, A&A, 431, 793
Villar-Martín, M., Vernet, J., di Serego Alighieri, S., et al. 2003, MNRAS, 346, 273
West, M. J. 1994, MNRAS, 268, 79
Willott, C. J., Rawlings, S., Blundell, K. M., Lacy, M., & Eales, S. A. 2001, MNRAS, 322, 536
Wold, M., Armus, L., Neugebauer, G., Jarrett, T. H., & Lehnert, M. D. 2003, AJ, 126, 1776
Zirm, A. W., Dickinson, M., & Dey, A. 2003, ApJ, 585, 90
Zirm, A. W., Overzier, R. A., Miley, G. K., et al. 2005, ApJ, 630, 68

Online Material

Appendix A: Object lists

Table A.1. Position and properties of the Lyα emission line of the confirmed Lyα emitters and the radio galaxy in the 2048 field.

Object	Position		z	Flux	EW_0	*FWHM*
	α_{J2000}	δ_{J2000}		erg s^{-1} cm^{-2}	Å	km s^{-1}
2048.LAE1	20 51 02.05	−27 04 52.7	2.1058 ± 0.0004	(1.5 ± 0.2)×10^{-16}	145^{+56}_{-35}	720 ± 70
2048.LAE2	20 51 07.53	−27 04 46.1	2.0591 ± 0.0005	(1.1 ± 0.1)×10^{-16}	37^{+4}_{-3}	1015 ± 115
2048.LAE3	20 51 13.26	−27 00 57.8	2.0580 ± 0.0005	(1.5 ± 0.8)×10^{-17}	23^{+6}_{-5}	<415
2048.RG	20 51 03.45	−27 03 04.1	2.0590 ± 0.0004	(2.9 ± 0.3)×10^{-16}	309^{+50}_{-27}	1580 ± 110

Table A.2. Position and properties of the Lyα emission line of the confirmed Lyα emitters and the radio galaxy in the 0052 field.

Object	Position		z	Flux	EW_0	*FWHM*
	α_{J2000}	δ_{J2000}		erg s^{-1} cm^{-2}	Å	km s^{-1}
0052.LAE1	00 54 14.83	−23 51 27.4	2.8301 ± 0.0010	(4.8 ± 0.5)×10^{-16}	104^{+6}_{-5}	1075 ± 85
0052.LAE2	00 54 15.01	−23 49 42.9	2.8655 ± 0.0003	(1.1 ± 0.2)×10^{-17}	76^{+1000}_{-21}	305 ± 50
0052.LAE3	00 54 19.05	−23 51 41.7	2.8359 ± 0.0002	(1.0 ± 0.3)×10^{-17}	9^{+4}_{-3}	155 ± 40
0052.LAE4	00 54 21.74	−23 51 51.1	2.8691 ± 0.0004	(4.4 ± 1.6)×10^{-17}	123^{+488}_{-25}	430 ± 50
0052.LAE5	00 54 21.95	−23 54 08.9	2.8666 ± 0.0002	(1.2 ± 0.2)×10^{-16}	443^{+156}_{-62}	220 ± 30
0052.LAE6	00 54 22.62	−23 55 07.0	2.8489 ± 0.0002	(1.8 ± 0.5)×10^{-17}	52^{+492}_{-13}	255 ± 40
0052.LAE7	00 54 22.75	−23 53 06.7	2.8599 ± 0.0002	(1.0 ± 0.3)×10^{-17}	94^{+24}_{-18}	205 ± 50
0052.LAE8	00 54 24.57	−23 53 12.8	2.8449 ± 0.0002	(2.0 ± 0.4)×10^{-17}	218^{+42}_{-28}	220 ± 40
0052.LAE9	00 54 24.58	−23 54 54.7	2.8636 ± 0.0004	(5.2 ± 2.3)×10^{-17}	49^{+27}_{-9}	525 ± 85
0052.LAE10	00 54 25.35	−23 53 07.5	2.8628 ± 0.0003	(4.2 ± 1.0)×10^{-18}	54^{+495}_{-14}	305 ± 50
0052.LAE11	00 54 25.64	−23 53 40.6	2.8448 ± 0.0001	(6.1 ± 1.1)×10^{-18}	105^{+24}_{-18}	130 ± 25
0052.LAE12	00 54 26.05	−23 51 40.6	2.8656 ± 0.0004	(2.7 ± 0.9)×10^{-18}	68^{+365}_{-16}	280 ± 80
0052.LAE13	00 54 27.31	−23 51 52.9	2.8651 ± 0.0008	(2.3 ± 0.6)×10^{-17}	114^{+33}_{-24}	765 ± 150
0052.LAE14	00 54 28.17	−23 51 52.3	2.8444 ± 0.0012	(1.0 ± 0.3)×10^{-17}	56^{+199}_{-12}	950 ± 235
0052.LAE15	00 54 28.59	−23 53 48.6	2.8550 ± 0.0002	(1.2 ± 0.1)×10^{-16}	108^{+26}_{-11}	585 ± 25
0052.LAE16	00 54 28.65	−23 51.55.3	2.8479 ± 0.0003	(2.1 ± 0.4)×10^{-17}	45^{+26}_{-8}	325 ± 50
0052.LAE17	00 54 28.89	−23 52 26.3	2.8673 ± 0.0004	(1.0 ± 0.2)×10^{-17}	26^{+9}_{-5}	395 ± 70
0052.LAE18	00 54 29.31	−23 53 18.1	2.8669 ± 0.0002	(5.2 ± 0.5)×10^{-17}	132^{+78}_{-19}	425 ± 30
0052.LAE19	00 54 29.84	−23 54 42.8	2.8618 ± 0.0001	(2.3 ± 0.3)×10^{-17}	168^{+1000}_{-39}	285 ± 30
0052.LAE20	00 54 30.53	−23 53 34.1	2.8592 ± 0.0003	(6.9 ± 2.6)×10^{-18}	78^{+22}_{-17}	150 ± 60
0052.LAE21	00 54 30.61	−23 53 36.2	2.8600 ± 0.0003	(7.2 ± 1.6)×10^{-18}	27^{+11}_{-5}	260 ± 50
0052.LAE22	00 54 31.99	−23 49 09.3	2.8503 ± 0.0002	(4.8 ± 0.8)×10^{-18}	118^{+26}_{-20}	225 ± 30
0052.LAE23	00 54 32.86	−23 52 14.1	2.8660 ± 0.0003	(1.1 ± 0.3)×10^{-17}	74^{+211}_{-16}	365 ± 65
0052.LAE24	00 54 34.64	−23 53 27.7	2.8460 ± 0.0004	(1.0 ± 0.3)×10^{-17}	76^{+21}_{-16}	275 ± 75
0052.LAE25	00 54 35.61	−23 53 27.9	2.8441 ± 0.0003	(1.7 ± 0.3)×10^{-16}	468^{+165}_{-65}	430 ± 50
0052.LAE26	00 54 35.66	−23 54 16.7	2.8602 ± 0.0002	(6.6 ± 2.3)×10^{-18}	34^{+34}_{-8}	90 ± 55
0052.LAE27	00 54 36.28	−23 50 01.6	2.8437 ± 0.0003	(2.0 ± 0.2)×10^{-17}	27^{+14}_{-6}	670 ± 60
0052.LAE28	00 54 36.30	−23 53 39.1	2.8451 ± 0.0010	(6.2 ± 2.6)×10^{-18}	115^{+46}_{-19}	610 ± 200
0052.LAE29	00 54 36.55	−23 53 40.2	2.8447 ± 0.0002	(4.8 ± 1.3)×10^{-18}	146^{+33}_{-23}	120 ± 40
0052.LAE30	00 54 37.13	−23 51 39.2	2.8647 ± 0.0003	(1.5 ± 0.6)×10^{-17}	102^{+31}_{-22}	145 ± 55
0052.LAE31	00 54 38.54	−23 48 39.8	2.8647 ± 0.0003	(6.4 ± 0.9)×10^{-17}	105^{+21}_{-10}	860 ± 50
0052.LAE32	00 54 39.91	−23 52 06.6	2.8311 ± 0.0003	(1.3 ± 0.3)×10^{-17}	410^{+130}_{-82}	495 ± 70
0052.LAE33	00 54 40.36	−23 49 13.1	2.8499 ± 0.0001	(4.8 ± 1.4)×10^{-18}	136^{+28}_{-21}	65 ± 40
0052.LAE34	00 54 42.46	−23 50 50.5	2.8663 ± 0.0004	(5.4 ± 1.3)×10^{-18}	101^{+1000}_{-25}	410 ± 75
0052.LAE35	00 54 42.90	−23 52 55.9	2.8756 ± 0.0003	(4.2 ± 0.5)×10^{-17}	165^{+1000}_{-39}	440 ± 35
0052.LAE36	00 54 43.06	−23 53 14.1	2.8764 ± 0.0004	(1.7 ± 0.3)×10^{-16}	28^{+3}_{-2}	590 ± 30
0052.LAE37	00 54 44.36	−23 51 52.4	2.8619 ± 0.0002	(1.1 ± 0.2)×10^{-17}	38^{+24}_{-8}	265 ± 45
0052.RG	00 54 29.83	−23 51 31.1	2.8609 ± 0.0011	(1.11 ± 0.09)×10^{-15}	133^{+6}_{-5}	2040 ± 85

Table A.3. Position and properties of the Lyα emission line of the confirmed Lyα emitters and the radio galaxy in the 0943 field.

Object	Position		z	Flux	EW_0	*FWHM*
	α_{J2000}	δ_{J2000}		erg s^{-1} cm^{-2}	Å	km s^{-1}
0943.LAE1	09 45 20.70	−24 28 12.5	2.8970 ± 0.0002	(3.1 ± 0.2)×10^{-17}	131^{+1000}_{-44}	600 ± 35
0943.LAE2	09 45 21.99	−24 29 55.1	2.9202 ± 0.0001	(2.2 ± 0.2)×10^{-17}	88^{+231}_{-16}	290 ± 25
0943.LAE3	09 45 22.17	−24 28 56.2	2.9259 ± 0.0002	(2.2 ± 0.2)×10^{-17}	144^{+11}_{-10}	425 ± 45
0943.LAE4	09 45 23.77	−24 28 48.0	2.9263 ± 0.0007	(6.7 ± 1.0)×10^{-17}	38^{+26}_{-6}	555 ± 75
0943.LAE5	09 45 27.14	−24 27 52.6	2.9167 ± 0.0005	(1.1 ± 0.3)×10^{-17}	61^{+9}_{-8}	360 ± 115
0943.LAE6	09 45 29.09	−24 26 49.7	2.9242 ± 0.0003	(1.3 ± 0.2)×10^{-17}	70^{+9}_{-8}	225 ± 75
0943.LAE7	09 45 30.60	−24 25 31.4	2.9265 ± 0.0005	(7.4 ± 1.8)×10^{-18}	9^{+6}_{-2}	455 ± 100
0943.LAE8	09 45 30.66	−24 28 06.2	2.9113 ± 0.0002	(4.7 ± 0.4)×10^{-17}	35^{+14}_{-5}	455 ± 35
0943.LAE9	09 45 30.83	−24 28 01.4	2.9214 ± 0.0006	(6.1 ± 2.1)×10^{-18}	8^{+14}_{-3}	410 ± 140
0943.LAE10	09 45 31.13	−24 27 34.4	2.9122 ± 0.0006	(1.0 ± 0.2)×10^{-17}	71^{+11}_{-10}	440 ± 65
0943.LAE11	09 45 32.26	−24 31 21.6	2.9259 ± 0.0003	(9.8 ± 1.4)×10^{-18}	49^{+319}_{-11}	445 ± 60
0943.LAE12	09 45 32.68	−24 29 46.5	2.9004 ± 0.0003	(2.1 ± 0.2)×10^{-16}	67^{+18}_{-10}	625 ± 30
0943.LAE13	09 45 32.77	−24 29 05.4	2.9189 ± 0.0003	(7.7 ± 0.8)×10^{-17}	103^{+569}_{-20}	630 ± 35
0943.LAE14	09 45 32.86	−24 31 06.9	2.9073 ± 0.0000	(4.1 ± 0.1)×10^{-17}	177^{+23}_{-19}	180 ± 10
0943.LAE15	09 45 34.34	−24 29 23.7	2.9094 ± 0.0001	(3.2 ± 0.2)×10^{-17}	111^{+1000}_{-26}	330 ± 20
0943.LAE16	09 45 34.96	−24 30 46.9	2.9242 ± 0.0002	(1.7 ± 0.2)×10^{-17}	28^{+9}_{-4}	275 ± 50
0943.LAE17	09 45 36.18	−24 30 00.5	2.9174 ± 0.0005	(1.7 ± 0.5)×10^{-17}	20^{+36}_{-5}	305 ± 90
0943.LAE18	09 45 36.36	−24 29 56.4	2.9313 ± 0.0002	(5.4 ± 0.3)×10^{-17}	133^{+418}_{-24}	695 ± 35
0943.LAE19	09 45 37.19	−24 26 27.2	2.9081 ± 0.0003	(2.8 ± 0.6)×10^{-17}	103^{+17}_{-14}	430 ± 45
0943.LAE20	09 45 37.52	−24 25 23.7	2.9266 ± 0.0005	(5.1 ± 0.6)×10^{-17}	165^{+12}_{-11}	720 ± 60
0943.LAE21	09 45 38.64	−24 29 54.3	2.9159 ± 0.0006	(2.2 ± 0.8)×10^{-17}	136^{+14}_{-12}	595 ± 80
0943.LAE22	09 45 38.71	−24 29 57.5	2.9201 ± 0.0003	(1.6 ± 0.2)×10^{-17}	20^{+6}_{-3}	510 ± 55
0943.LAE23	09 45 39.08	−24 30 10.2	2.9189 ± 0.0004	(5.6 ± 1.3)×10^{-17}	33^{+20}_{-6}	680 ± 65
0943.LAE24	09 45 39.17	−24 29 20.1	2.9089 ± 0.0002	(2.1 ± 0.2)×10^{-17}	26^{+19}_{-6}	515 ± 40
0943.LAE25	09 45 39.46	−24 26 15.9	2.9037 ± 0.0010	(2.0 ± 0.4)×10^{-17}	221^{+42}_{-30}	1185 ± 195
0943.LAE26	09 45 41.88	−24 28 35.1	2.9309 ± 0.0008	(4.3 ± 1.9)×10^{-18}	7^{+5}_{-2}	360 ± 165
0943.LAE27	09 45 42.61	−24 28 57.9	2.9302 ± 0.0001	(2.1 ± 0.2)×10^{-17}	150^{+1000}_{-32}	285 ± 25
0943.LAE28	09 45 45.72	−24 26 49.1	2.9233 ± 0.0007	(3.1 ± 0.7)×10^{-17}	86^{+477}_{-17}	630 ± 60
0943.RG	09 45 32.74	−24 28 49.7	2.9209 ± 0.0003	(3.6 ± 0.1)×10^{-15}	173^{+3}_{-3}	1755 ± 20

Table A.4. Position and properties of the Lyα emission line of the confirmed Lyα emitters and the radio galaxy in the 2009 field.

Object	Position		z	Flux	EW_0	*FWHM*
	α_{J2000}	δ_{J2000}		erg s^{-1} cm^{-2}	Å	km s^{-1}
2009.LAE1	20 09 38.32	−30 41 31.6	3.1528 ± 0.0001	(7.2 ± 0.7)×10^{-18}	75^{+10}_{-8}	175 ± 20
2009.LAE2	20 09 39.89	−30 40 50.7	3.1577 ± 0.0007	(2.6 ± 0.8)×10^{-18}	12^{+20}_{-4}	530 ± 135
2009.LAE3	20 09 40.92	−30 41 44.9	3.1548 ± 0.0006	(1.6 ± 0.6)×10^{-18}	25^{+206}_{-6}	385 ± 115
2009.LAE4	20 09 41.06	−30 42 46.4	3.1415 ± 0.0005	(1.9 ± 0.7)×10^{-18}	73^{+11}_{-9}	320 ± 95
2009.LAE5	20 09 42.19	−30 38 34.3	3.1601 ± 0.0003	(4.2 ± 0.7)×10^{-18}	16^{+52}_{-6}	370 ± 50
2009.LAE6	20 09 47.83	−30 42 39.6	3.1521 ± 0.0004	(1.4 ± 0.2)×10^{-17}	27^{+50}_{-6}	720 ± 75
2009.LAE7	20 09 49.55	−30 40 47.4	3.1531 ± 0.0003	(1.7 ± 0.4)×10^{-17}	23^{+37}_{-5}	485 ± 55
2009.LAE8	20 09 54.43	−30 41 19.7	3.1445 ± 0.0006	(1.4 ± 0.4)×10^{-16}	38^{+699}_{-10}	505 ± 120
2009.LAE9	20 09 56.94	−30 39 38.6	3.1412 ± 0.0006	(6.5 ± 0.3)×10^{-16}	49^{+4}_{-3}	3170 ± 50
2009.LAE10	20 09 58.82	−30 40 37.1	3.1454 ± 0.0004	(7.3 ± 0.3)×10^{-16}	84^{+14}_{-8}	1565 ± 25
2009.LAE11	20 10 01.81	−30 41 27.7	3.1581 ± 0.0003	(5.8 ± 0.5)×10^{-17}	23^{+6}_{-3}	750 ± 30
2009.RG	20 09 48.12	−30 40 07.4	3.1497 ± 0.0002	(2.41 ± 0.04)×10^{-15}	68^{+1}_{-1}	2300 ± 25

Table A.5. Position and properties of the Lyα emission line of the confirmed Lyα emitters and the radio galaxy in the two 1338 fields.

Object	Position		z	Flux	EW_0	$FWHM$
	α_{J2000}	δ_{J2000}		erg s^{-1} cm^{-2}	Å	km s^{-1}
1338.LAE1	13 38 21.27	−19 45 52.7	4.0977 ± 0.0010	(1.5 ± 0.4)×10^{-17}	55^{+38}_{-7}	495 ± 105
1338.LAE2	13 38 21.32	−19 44 42.5	4.1092 ± 0.0003	(8.1 ± 2.2)×10^{-18}	33^{+17}_{-6}	<255
1338.LAE3	13 38 21.68	−19 46 27.9	4.0978 ± 0.0003	(1.0 ± 0.4)×10^{-18}	14^{+7}_{-3}	75 ± 75
1338.LAE4	13 38 22.47	−19 44 33.8	4.0950 ± 0.0002	(2.7 ± 0.3)×10^{-17}	51^{+7}_{-4}	230 ± 40
1338.LAE5	13 38 22.78	−19 46 04.8	4.0976 ± 0.0003	(3.0 ± 1.1)×10^{-18}	49^{+16}_{-13}	120 ± 65
1338.LAE6	13 38 23.65	−19 45 51.7	4.0969 ± 0.0003	(2.2 ± 0.7)×10^{-18}	24^{+5}_{-3}	95 ± 55
1338.LAE7	13 38 24.79	−19 41 34.2	4.1055 ± 0.0004	(5.9 ± 1.4)×10^{-18}	29^{+51}_{-7}	<260
1338.LAE8	13 38 24.87	−19 41 46.0	4.1017 ± 0.0007	(9.2 ± 2.9)×10^{-18}	31^{+23}_{-6}	270 ± 140
1338.LAE9	13 38 25.11	−19 43 11.2	4.1004 ± 0.0007	(7.0 ± 1.3)×10^{-17}	63^{+15}_{-7}	720 ± 55
1338.LAE10	13 38 25.32	−19 45 55.9	4.0970 ± 0.0002	(1.6 ± 0.3)×10^{-17}	167^{+25}_{-17}	420 ± 90
1338.LAE11	13 38 26.18	−19 43 34.7	4.1010 ± 0.0006	(6.0 ± 1.5)×10^{-17}	70^{+23}_{-9}	445 ± 45
1338.LAE12	13 38 26.20	−19 46 28.5	4.0925 ± 0.0005	(9.0 ± 1.7)×10^{-18}	152^{+32}_{-22}	460 ± 55
1338.LAE13	13 38 28.08	−19 39 50.5	4.0877 ± 0.0004	(1.4 ± 0.4)×10^{-17}	278^{+1000}_{-62}	<170
1338.LAE14	13 38 28.73	−19 44 37.2	4.1020 ± 0.0002	(4.5 ± 0.6)×10^{-17}	123^{+1000}_{-18}	<200
1338.LAE15	13 38 29.41	−19 49 01.7	4.1010 ± 0.0005	(2.5 ± 0.6)×10^{-18}	80^{+22}_{-15}	405 ± 75
1338.LAE16	13 38 29.68	−19 44 00.0	4.1021 ± 0.0003	(4.6 ± 1.2)×10^{-18}	31^{+9}_{-4}	<165
1338.LAE17	13 38 29.88	−19 43 26.1	4.0927 ± 0.0004	(7.0 ± 1.3)×10^{-18}	267^{+1000}_{-71}	350 ± 80
1338.LAE18	13 38 30.16	−19 40 38.3	4.1132 ± 0.0005	(1.6 ± 0.4)×10^{-17}	98^{+391}_{-19}	275 ± 105
1338.LAE19	13 38 30.17	−19 48 44.9	4.0872 ± 0.0003	(7.1 ± 1.2)×10^{-18}	144^{+1000}_{-37}	240 ± 35
1338.LAE20	13 38 32.85	−19 44 07.2	4.0969 ± 0.0003	(7.6 ± 1.8)×10^{-18}	45^{+30}_{-6}	<170
1338.LAE21	13 38 33.58	−19 43 36.3	4.0965 ± 0.0009	(4.6 ± 0.9)×10^{-17}	31^{+3}_{-2}	380 ± 80
1338.LAE22	13 38 34.15	−19 42 53.4	4.0955 ± 0.0009	(2.6 ± 0.8)×10^{-17}	42^{+105}_{-9}	505 ± 150
1338.LAE23	13 38 34.44	−19 47 03.7	4.0983 ± 0.0003	(3.7 ± 0.8)×10^{-18}	66^{+348}_{-13}	215 ± 45
1338.LAE24	13 38 34.69	−19 43 43.2	4.0979 ± 0.0002	(3.3 ± 0.6)×10^{-18}	35^{+301}_{-6}	135 ± 30
1338.LAE25	13 38 34.98	−19 42 25.4	4.0925 ± 0.0008	(7.4 ± 2.6)×10^{-18}	19^{+7}_{-4}	275 ± 160
1338.LAE26	13 38 35.10	−19 45 07.8	4.0967 ± 0.0005	(5.4 ± 2.3)×10^{-18}	53^{+18}_{-13}	<150
1338.LAE27	13 38 35.52	−19 45 23.7	4.0999 ± 0.0005	(9.4 ± 2.3)×10^{-18}	90^{+420}_{-15}	230 ± 110
1338.LAE28	13 38 35.67	−19 45 50.1	4.0987 ± 0.0003	(3.1 ± 0.7)×10^{-18}	54^{+14}_{-9}	395 ± 70
1338.LAE29	13 38 35.82	−19 49 36.5	4.0975 ± 0.0004	(3.5 ± 0.9)×10^{-18}	27^{+5}_{-3}	335 ± 70
1338.LAE30	13 38 37.15	−19 45 02.0	4.0943 ± 0.0003	(6.0 ± 1.0)×10^{-17}	103^{+141}_{-12}	440 ± 35
1338.LAE31	13 38 39.69	−19 47 50.1	4.0948 ± 0.0007	(3.6 ± 1.0)×10^{-17}	72^{+32}_{-10}	575 ± 45
1338.LAE32	13 38 41.10	−19 43 01.7	4.0941 ± 0.0007	(2.3 ± 0.2)×10^{-16}	16^{+1}_{-1}	2110 ± 85
1338.LAE33	13 38 41.11	−19 44 22.4	4.1015 ± 0.0005	(1.9 ± 0.6)×10^{-17}	49^{+17}_{-13}	235 ± 75
1338.LAE34	13 38 43.85	−19 44 41.0	4.0978 ± 0.0003	(2.4 ± 0.6)×10^{-17}	101^{+1000}_{-26}	220 ± 30
1338.LAE35	13 38 44.65	−19 47 09.4	4.1185 ± 0.0002	(3.2 ± 0.3)×10^{-17}	313^{+1000}_{-53}	300 ± 40
1338.LAE36	13 38 47.19	−19 48 16.7	4.0979 ± 0.0008	(1.8 ± 0.4)×10^{-17}	119^{+25}_{-18}	655 ± 125
1338.LAE37	13 38 50.12	−19 46 12.2	4.0958 ± 0.0004	(1.2 ± 0.4)×10^{-18}	37^{+52}_{-8}	165 ± 55
1338.RG	13 38 26.06	−19 42 30.8	4.1052 ± 0.0006	(4.4 ± 0.2)×10^{-15}	578^{+16}_{-14}	1810 ± 40